Geothermal Reconnaissance: Remote Sensing and GIS Applications in the Investigation of Thermal Anomalies Near Trinidad, Colorado

Jennifer Alexis-Brooke Bloom
Department of Geography, University of Colorado at Boulder

Defense Date: November 3, 2015

Thesis Advisor:
Dr. Waleed Abdalati, Department of Geography

Defense Committee:
Honors Council Advisor: William Travis, Department of Geography
Committee Member: Suzanne Nelson, Department of Integrated Physiology

Abstract

The focus of this thesis is to explore remote sensing and GIS techniques used in the exploration of geothermal energy resources. A literature review investigated various methodologies, workflows, and algorithms used in geothermal reconnaissance. This knowledge was then implemented in a case study of regions in Colorado. Using GIS data and maps, a region showing high potential of geothermal resource presence was determined. Located near Trinidad, Colorado, this region of interest was then investigated through image analysis incorporating methods researched in the literature review. Anomalies were found and confirmed complications found in current practices in remote sensing geothermal resources. Thermal infrared (TIR) analysis is complicated with introduced thermal noise from insolation interactions with both surface and atmosphere, resulting in a masking of subsurface thermal anomalous readings. Further research is required to remove the effects of insolation to create an efficient geothermal reconnaissance workflow. This workflow would be improved with the incorporation of *in situ* spectroscopic analysis used in tandem with hyperspectral and high resolution shortwave infrared (SWIR) image analysis methodologies accounting for insolation and thermal inertia effects. Field work obtaining thermal and mineralogical spectroscopy of regions with discovered anomalies using GIS data and interpolated map surfaces will improve workflow. Incorporating field data covering a region of interest over time, observing seasonal changes in solar radiation and precipitation can improve landcover classification techniques and improve the location of geothermal resources.

Table of Contents:

Introduction

The purpose of this paper is to analyze the use of remote sensing platforms and techniques in the exploration and reconnaissance of geothermal energy resources, with the intent of advancing renewable energy development and electrical exploitation. The advantages geothermal heat offers as a renewable energy resource to generate electricity are profound. Geothermal energy production produces considerably less greenhouse gas emissions in comparison to fossil fuel technologies, with the only direct emissions being those coming from underground hydrothermal fluids, at volumes similar to hydropower (Goldstein et al. 2011; Kristmannsdóttir and Ármannsson 2003). Electricity generated by geothermal is around 10-17%, or roughly three times less efficient than electricity generated by nuclear or coal power plants, primarily because of steam temperatures, but Enhanced Geothermal Systems will be developed with improved efficiency and zero direct emissions (Barbier 2000; Goldstein et al. 2011). In spite of this reduced efficiency, geothermal energy is unique in comparison to other renewables like wind and solar, because it can provide consistent base-loads of electricity annually (Goldstein et al. 2011; Renewable Energy Data Book, 2014). When developing geothermal for electricity production, the identification, classification and drilling of geothermal fields accounts for half the cost of investment; geothermal-electric projects have high upfront costs, but relatively low costs of electricity once developed (Barbier 2000; Goldstein et al. 2011). Reducing this cost is imperative to the goal of developing more sustainable energy infrastructure, ultimately establishing an energy system that will contribute to long term greenhouse gas emissions (Goldstein et al. 2011).

To form a foundation on geothermal remote sensing methods, a literature review was conducted and focused on citations highlighting articles and papers regarding remote sensing

applications that improves confirmation of *in situ* ground data. Current practices in remote sensing geothermal resources often rely on thermal infrared (TIR) imagery (van der Meer et al. 2014). However, methods involving TIR image analysis are complicated and time consuming because of introduced thermal noise from both surface and atmosphere, masking subsurface thermal anomalous readings (Coolbaugh et al. 2007). To compensate for this complexity, an integrated methodology combining Geographic Information Systems (GIS) with remotely sensed imagery and localized surface information is required, in the hopes of broadening this methodology to utilize earth observation data from many platforms with different specifications. A case study of specific regions in Colorado was conducted using funds from the von Dreden Fellowship to research and compare various remotely sensed methods for geothermal reconnaissance. To locate regions of higher geothermal energy potential, GIS data derived from field measurements found in the drilling of oil, gas, and exploratory wells was obtained from the Colorado Geological Survey (CGS) (Berkman and Carroll 2008). These top tier regions are explored using imagery from the Advanced Spaceborne Thermal Emission and Reflection Radiometer (ASTER) instrument onboard the *Terra* platform.

If a successful method is found through the case study, it will save time, providing a workflow for future remote sensing techniques in geothermal resource exploration. If such a method proves unsuccessful, future analysts will also be saved time by not using this method. Ultimately, by researching a combination method of remote sensing and GIS techniques, the accuracy of remotely sensed geothermal exploration will be refined.

Literature Review

Geology

Colorado is home to the Rio Grand rift, a north-trending continental rift zone comprised of several basins, including the northernmost San Luis Basin and the Raton Basin near Trinidad, Colorado (Chronic and Williams 2002). The rift is experiencing extensional tectonics, where crustal rock slowly stretches and separates, forming faults and deformations (Wilson et al. 2005). This generates a thinner crust where the asthenosphere has intruded into the lithosphere and crust, producing volcanic intrusions along the Rio Grande rift, such as the Raton-Claton Volcanic Field in New Mexico (Chronic and Williams 2002; Gao et al. 2004; Wilson et al. 2005). These regions around the San Luis Basin, including the San Juan Mountain extrusive complex and the western Raton Basin, carry high oil and gas potential. The extrusive volcanics of the rift generate geothermal anomalies and helped produce the high-ranking coal beds in the region that also possess large volumes of methane gas (Choate et al. 1982). Geothermal field systems frequently occur within calderas and graben-like depressions, such as land between two faults or rift valleys, and these geothermal systems are commonly associated with Northwest and Northeast trending faults (Carranza et al. 2008b). For these reasons, areas near the Rio Grande rift were selected for further analysis in a case study.

Geothermal Energy

Geothermal energy is an endogenic form of heat that moves via conduction and convection processes from the mantle outward toward the Earth's crust. The energy results from the upward movement of magma, forming pockets in the mantle. These magma pockets heat the crust as well as groundwater reservoirs. As thermal energy heats the water, steam is generated.

The hot water and steam move upward, manifesting on the surface as hot springs, fumaroles, and steam vents. Geothermal energy can be harnessed at these specific surface locations to generate power. Although geothermal energy is a nearly limitless resource, few regions exist where the geothermal gradient is above average and anomalous, and at a depth shallow enough to be accessed by drilling.

Geothermal fields are locations at which subsurface magmatic activity causes anomalous temperature readings at or near the surface. The geothermal heat gradient transfers energy upward from Earth's interior to the surface through a medium, either dry rock or groundwater. The geothermal gradient is medium dependent, and different mediums have varying heat fluxes, or heat flow rates through the medium.

Geothermal systems have been classified into six categories: volcanic, magmatic, sedimentary, geopressured, hydrothermal, and hot dry rock (HDR). The most commonly exploited of these is the hydrothermal system, where the groundwater can exceed temperatures of 150°C (Barbier 2002). Each of these systems have unique heat flux characteristics that enable the grouping of these reservoirs into their functionality for resource extraction. For example, HDR mediums where the medium's geothermal gradient is anomalously high are suitable for creating man-made reservoirs using hydraulic fracturing, as water may not be natively present. These unique characteristics are also classifiable variables that are measurable using remote sensing. Geothermal prospecting through remote sensing and GIS methodologies can confirm the existence of geothermal fields that could be favorable for energy production. Remote sensing and GIS can also reduce costs involved in exploratory drilling by reducing drill sites to areas designated most thermally productive through more precise maps of field boundaries.

Quantifying what thermal energy is subsurface in origin as opposed to solar in origin is important in geothermal resource exploration; here remote sensing techniques can be utilized. As radioactive decay is conducted upward from the planet's interior, geothermal heat begins to convect as it nears the surface and begins to interact with surface heat generated by incoming solar radiation. Earth's geothermal temperature gradient is variable and dependent on distance from a location of volcanic or tectonic activity. Generally, the average temperature gradient is between 25-30°C per kilometer of depth; temperatures increase as depth increases. This value is represented as being a conductive heat flux of 0.1 MW/km^2 (Van der Meer 2014).

In areas of shallow depth with above average gradients, magmatic activity could be the source of heat. In this case, magma bodies close to the surface are undergoing a phase change from plasma to solid, and this cooling is releasing heat (Barbier 2002). An increasing geothermal temperature gradient can originate from nearby geologically active regions such as at diverging or converging plate boundaries such as rifts, and at volcanically active intraplate systems such as hot spots. Colorado has high potential for producing electricity through geothermal power because the state has the second most highest and aerially extensive heat flow anomalies in the United States (Sares et al. 2009). One of the regions of interest noted in Colorado as having high potential for geothermal power plant sites is the Raton Basin, where wells have geothermal gradients greater than 50°C/km (Sares et al 2009). Here, traditional geothermal and hydrothermal energy methods could be implemented, as could EGS technologies to utilize resources at depths up to 30,000 ft down (Sares et al. 2009).

Shallow hydrothermal systems are defined at existing at depths of 6,500-11,000ft. Hydrothermal reservoirs develop when surface water percolates into the crust from porous

recharge areas, generating an underground aquifer (Barbier 2002). The rock's porosity enables the aquifer's recharge, and enables circulating hot water to move upward, where convected heat energy dispels at the surface through vents and exposed hot springs. Often, the aquifer is under pressure because its porous recharge area is capped with an impermeable surface, preventing the water from being released. As water is an excellent heat absorber, it carries and stores the geothermal heat in a liquid, gaseous, or mixed state. High pressures often prevail within the thermal reservoir with persisting temperatures often above 300°C (Barbier 2002). Eventually, this temperature and pressure is released via steam vents, fumaroles or hot springs, or can also be accessed via a drilled well, depending on the reservoir's depth.

Deeper geothermal resource depths can exist at 10,000-30,000 feet into the crust, however, application of geothermal energy for electrical energy production at these depths is dependent on Enhanced Geothermal Systems (EGS) development (Sares et al. 2009). As noted earlier, thermal reservoirs can be synthetically produced through the injection of fluids (Ziagos et al. 2013). Enhanced Geothermal Systems can generate electricity from geothermal energy without natural convective hydrothermal resources.

Until recently, geothermal power systems have only exploited resources where naturally occurring heat, water, and rock permeability are sufficient and shallow enough to allow energy extraction. However, most of geothermal energy within reach of conventional techniques is in dry and impermeable rock. EGS technologies can enhance or create geothermal resources in this previously unsuitable hot dry rock (HDR) through hydraulic stimulation (Sares et al. 2009). Unfortunately, public concern has hindered the development of EGS because of the potential impacts of induced seismicity during development (Majer et al. 2007). Case studies have been

conducted showing EGS-induced seismicity does not need to conflict with geothermal energy resource development. The seismicity can provide beneficial insight into geothermal reservoir processes monitoring, and provided site selection is carried out with proper infrastructure, knowledge, and community cooperation, EGS-induced seismicity can be better mitigated and understood (Majer et al. 2007).

Current Methods of Geothermal Exploration

Remote sensing data is often used to locate and research geothermal fields, and has been historically utilized by geologists for regional mapping since its inception (van der Meer et al. 2012). Field methods act to validate remote sensing techniques. Traditional exploratory methods have involved various geological surveys where wells are drilled to determine if resource capacities are present at a given location. Ground surveys often inventory many characteristics, including surface topographic deformation, chemistry, temperature, flow-rates, gas composition, and other geophysical properties including electromagnetic properties, gravity and electrical resistivity. This data is often compiled and modeled to predict geothermal heat flow rates at the sites (Barbier 2002). Similar methods were used by the Colorado Geological Survey to create the maps used in this paper's case study. Traditional geological surveys aid in integration of remote sensing methods by temporally and spatially validating sensor data. Ancillary *in situ* data is best integrated through a Geographic Information System. This method has been used to prioritize resource extraction and site development by determining site appropriation through Boolean logic and index overlays (Noorollahi et al. 2007).

Variables indicating geothermal activity have geometric, morphological and radiometric characteristics. Examples of these variables include hydrothermal geochemistry, gaseous

emissions, mineralogical facies, surface geomorphology, geobotanical indicators, and thermal anomalous subsurface readings from *in situ* radar field measurements, to name a few. Remote sensing is often used in geothermal research to explore these variables. Techniques implemented depend on the specific geothermal region in question, and for each variable, certain sensors are preferred and often used (van der Meer et al. 2014). These variables act as either direct or indirect evidence of geothermal energy in remote sensing geothermal methodologies. Techniques are grouped in accordance to the variable they investigate: surface deformation, gaseous emissions, structural analysis, mineral mapping, surface temperature mapping, heat flux mapping, and geobotanical analysis. Ancillary data gathered via *in situ* measurements act as validation of remotely sensed data that indicates evidence of subsurface geothermal activity (van der Meer et al. 2014).

Techniques involving the use of these variables in geothermal reconnaissance are numerous. For example, hyperspectral spectrometry is used to locate and map reflectance and emissivity signatures of geothermal indicator minerals (Kruse 2012). Mineral spectroscopy in the visible and infrared wavelengths enable detection of minerals that are indicative of geochemical weathering processes marking the presence of hydrothermal activity (Carranza et al. 2008a; Huntington 1996). Regional mineralogy, topography, and gaseous chemistry are investigated in the visible, near, shortwave and longwave infrared wavelengths. This is done using analysis of hyperspectral, Interferometric Synthetic Aperture Radar (InSAR), Light Detection and Ranging (LiDAR), and digital elevation model (DEMs) imagery (Bateson et al. 2008; Carnec and Fabriol 1999; Kruse 2012). Principle Components Analysis (PCA) is a statistical processing technique that can enhance the spectral reflectance of specific minerals by subduing irradiance effects

across many bands. This was used on ASTER and Landsat ETM+ imagery to locate hydrothermal mineral deposits indicative of subsurface resources, such as gold, and can also be used to locate geothermal activity (Crosta et al. 2003). Geochemical ground surveys catalog gaseous content of thermal spring water and steam and are used as ancillary GIS data, combined with imagery (Arnórsson et al. 2006; Carranza et al. 2008a). Remote sensing techniques using infrared imagery and LiDAR analyze carbon dioxide degassing geochemistry and soil gas concentrations, for vent detection and vegetation health in proximal relation to geothermal activity (Noomen and Skidmore 2009; Tank et al. 2008). The hyperspectral classification of stressed and damaged vegetation showing increased reflectance in the 400-700nm wavelengths acts as a geobotanical indicator of thermal anomalies (Nash et al. 2003). Radar is also used for subsurface structural analysis, such as monitoring subsistence, and in discovering mineral deposits and textures indicating the presence of hydrothermal fields (Carnec and Fabriol 1999; Huntington 1996).

Another example of the use of remote sensing in geothermal exploration is seen in the investigation of hot spring mineral chemistry. Geothermal fluids have caustic chemical compositions that will dissolve minerals in the rock, altering surface substrate geochemistry. Surface rocks are often transformed into calcite, clays, or zeolites - porous aluminosilicate minerals, all of which are termed *sinter* (Barbier 2002). Sinter is formed as geothermal heat and pressure warp rock into these tempered alternative forms. Sinter is both a topographic and chemical indicator of subsurface temperature anomalies and hydrothermal aquifer chemistry (Haselwimmer and Prakash 2013). Such deposits can be classified using *in situ* spectroscopy, and hyperspectral and multispectral platforms, as all minerals possess unique spectral signatures

that can be located spectroscopically, particularly in the visible and shortwave infrared wavelength region of 0.4 - 2.5μm (Haselwimmer and Prakash 2013). Minerals such as hydroxyl bearing clays, sulfates, carbonates and sinter all have spectral absorption features that make these good indicators of hydrothermal alteration (Huntington 1996).

Another example of remote sensing techniques used in geothermal reconnaissance involves using the thermal and shortwave infrared bands of the Enhanced Thematic Mapper Plus (ETM+) sensor onboard the Landsat 7 platform. The availability of the Landsat missions has prompted their adoption in cost-effective geothermal reconnaissance development due to their relatively high spatial and temporal resolution, especially the later platforms, Landsat 7 ETM+ and Landsat 8, that possess thermal infrared sensors (one and two TIR bands, respectively). The use of Landsat 7 ETM+ for locating geothermal anomalies found in land surface temperatures of the thermal fields in Tengchong, China was the basis for this paper's case study (Qin et al. 2011). TIR data is used as a cost-effective analysis to scout resources and assist in the planning of geothermal ground surveys; this cost-effectiveness is expected to increase as TIR sensors onboard Unmanned Aerial Vehicles (UAVs) become increasingly available, providing high spatial resolutions when monitoring and mapping discrete geothermal systems and their surface formations, providing approximations of heat flow rates (Haselwimmer and Prakash 2013).

One of the largest constraints of TIR method applications in detecting subsurface thermal anomalies are surface-based thermal signals that insulate and mask anomalous readings, producing background thermal noise in TIR imagery. A method processing ASTER TIR imagery of Brady Hot Springs, Nevada, removed background diurnal thermal noise introduced by insolation (Coolbaugh et al 2007). Day and evening radiative heat energy images were generated

using an ENVI shaded relief tool that took solar effects with surface albedo and topographic slope into account. These were iteratively subtracted from an ASTER TIR image to better detect temperatures with subsurface origins. To produce a scaling factor, different constants for surfaces of varying thermal inertias were generated, and these heat energy images were then subtracted from the ASTER TIR imagery. Day and night images produced after subtraction were then combined with the weighted factors used to minimize thermal inertia, generating a final single image that quantified temperature anomalies. By accounting for background temperatures resulting from thermal inertia, surface albedo, and topographic slope and aspect, scene thermal variance was reduced by 30-50%. The resulting temperature differences that remained were from variations in geothermal heat flux (Coolbaugh et al. 2007).

Freek van der Meer, a renowned doctor in the field of geothermal remote sensing, notes there are "no integrated studies combining surface information from remote sensing with subsurface data and ancillary data sets" (van der Meer et al 2014, 267). He suggests combining surface information data sets using traditional *in situ* derived geothermal prospecting data alongside reservoir modeling enhanced with earth observation data. He suggests case study in which regional reconnaissance with multispectral sensors focus attention on localized areas possessing higher probabilities of geothermal resource availability. The Advanced Spaceborne Thermal Emission and Reflection Radiometer (ASTER) is good for this multispectral analysis because of its higher spectral and spatial resolutions, and its combination of visible and near infrared (VNIR), short wave infrared (SWIR) and thermal infrared (TIR) bands. ASTER possess three bands in VNIR with 15 m^2 spatial resolution, six bands that monitor the SWIR wavelengths at 30 m^2 spatial resolution, and five bands in the TIR wavelengths with 90 m^2 spatial resolution

(van der Meer, 2012). ASTER is also used in producing Digital Elevation Model (DEMs) alongside its near and shortwave infrared bands; this enables easy production of mineral indices when undergoing mineral mapping image processing. The Moderate Resolution Imaging Spectroradiometer (MODIS) can be used in long-term temporal monitoring of known geothermal locations (Vaughan et al. 2012). Although MODIS has a very coarse spatial resolution of 1 km^2 in the TIR bands, its temporal resolution is high, with daily revisitation to a region in comparison to ASTER's 16-day temporal resolution (van der Meer et al. 2012). Because of this high temporal resolution, MODIS can improve the spacial and temporal understanding of geothermal systems and their heat flux changes through time, such as allowing for improved monitoring of current geothermal resources to predict development or mitigate problems subsurface changes can present to infrastructure, and to validate land surface temperature retrieval from other platforms such as Landsat ETM+ (Qin et al. 2012; Rogan and Chen 2007; Vaughan et al. 2012). Hyperspectral sensors such as Airborne Visible/Infrared Imaging Spectrometer (AVIRIS) and NASA's EO-1 Hyperion sensor can be employed to map surface mineralogy, geobotanical indicators, and geothermal surface deformation using spectral analysis of unique spectral signatures present in these variables (Kruse 2012; van der Meer et al. 2012). Hyperion has very high spectral resolution, with 220 bands covering a 0.4-2.5μm spectral range, and has moderate spatial resolution at 30 m^2 that easily pairs with imagery from the Landsat platforms (van der Meer et al. 2012). AVIRIS sits onboard a Twin Otter aircraft platform and has 224 channels covering 0.4-2.5 μm in the electromagnetic spectrum at a high spatial resolution of 20 m pixels with 10.5 km swath with (Kruse 2012). Platforms such as these allow applications in VNIR-SWIR bands for mapping surface geology and topography. This can be used in tandem with the

TIR instrument mapping surface temperatures provide a good starting point for sensor integration methodologies (van der Meer et al. 2014). It is the intent of this paper's case study to begin exploration of a methodology that fits van der Meer's proposed suggestion.

Methodology

Literature Review

A comprehensive literature review on methods of geothermal remote sensing reconnaissance was conducted in order to understand the current state of reconnaissance, and to support exploration of combined methods through a case study. The literature review focused on core papers discussing geothermal energy and geothermal exploration, with emphasis on traditional methods that also incorporate image analysis. Other direct and indirect methods for locating geothermal anomalies were investigated. The sensors often used for this type of analysis were explored to select which sensor was the best fit for a case study of Colorado's geothermal anomaly potential. A method generated by Qin *et al.* for their detection of geothermal fields in Tengchong, China, was settled on as the backbone for the case study of Colorado's geothermal potential. The authors developed thermal infrared remote sensing techniques and algorithms using Landsat ETM+ thermal sensors to retrieve anomalous land surface temperatures (LST) of their study area. This was done by incorporating radiometric calibration, atmospheric correction, and emissivity calculation processes to determine LST. It was believed that Qin *et al.* methodology could be easily transferred and applied to different thermally sensed imagery, such as ASTER Level-1B imagery, however, this was not the case. As a result, the methodology's specific algorithms were unsuitable as a foundation for image processing, so the methodology

was revised to best suit the ASTER thermal sensors and their use in retrieving land surface temperature (LST) anomalies. The fundamental steps of the Qin *et al.* LST methodology utilizing radiometric calibration, atmospheric correction, and emissivity calculation was used to guide the case study, but was amended to suit the particular images and their specific constraints.

GIS-based predictive mapping has been used to initiate geothermal reconnaissance. Certain geologic features such as lithology, mineralogy, or structural formations are indicators of geothermal activity, and have a positive correlation indicating a spatial relationship between certain surface deformations and subsurface geothermal activity (van der Meer et al. 2014, 261-262). GIS modeling that used data from traditional methods of exploration accurately predicted 94% of the geothermal occurrences in a geothermal field in West Java, Indonesia (Carranza et al. 2008b). A weights-of-evidence logistic regression model using specific geologic information such as gravity gradients and earthquakes as unbiased evidence layers was also used to quantify geothermal resources and geospatially account for past explorations; the logistic regression model predicted the 33 known geothermal systems to 32.8 +/- 0.3 accuracy (Coolbaugh et al. 2005). Logistic regression is a statistical method used in modeling the probability of occurrence of a specific type of variable, such as a mineral deposit, in a given area; multivariate logistic regression has been successively used to produce evidence maps of ore deposits (Carranza et al. 2008a; Chung and Agterberg 1980). By relying on past exploratory data of interpolated geothermal heat flow and geothermal gradient modeling from previous geologists, a region of interest was in Colorado was found for further image analysis (Berkman and Carroll 2008).

Preliminary GIS Analysis for Image Selection

The Colorado Geological Survey (CGS) had created several predictive maps that were used to locate a region of interest. One such map was the *Interpretive Geothermal Heat Flow Map of Colorado*, created in October 2007 (Berkman and Carroll 2008). This map compiled heat flow data from several database resources, such as datasets from Southern Methodist University, University of North Dakota, and University of Michigan. This was combined with heat flow data collected and generated from temperature-depth logs in the field. The compiled parameters for each drill hole incorporated heat flow values, geothermal gradient, and thermal conductivities, but excluded original down-hole temperature-depth numbers. The CGS supplemented this data with 40 temperature-depth logs, thermal spring and well temperatures and additional published data to interpolate a surface using a least-squares best-fit linear equation to estimate Colorado's Heat Flow (Berkman and Carroll 2008).

By relying on past exploratory data of interpolated geothermal heat flow and geothermal gradient modeling from previous geologists, a region of interest in Colorado was found for further image analysis. Maps used were the most current offered by the Colorado Geological Survey. Additional GIS resources were also used in the selection of a region of interest, including data layers used in the formation of the "Interpretive Geothermal Gradient Map of Colorado," and the "Oil and Gas Wells in Areas of Colorado with Superior Geothermal Properties" map (Berkman and Carroll 2008; Berkman and Morgan 2010). The geothermal gradient data compiled to generate the interpretive gradient map incorporating CGS geothermal publications, global and national heat flow databases, and Colorado oil and gas well data. The map of wells with superior geothermal properties establishes locations of oil and gas wells in Colorado that

have good potential in re-opening for the purposes of geothermal resource sequestration. This map used data uploaded from the Colorado Oil and Gas Conservation Commission's database on June 4, 2009. Well locations were assigned geothermal properties using the interpolated gradient and heat flow zones from the "Interpretive Geothermal Heat Flow Map of Colorado." In tandem with well status codes, wells were graded on their potential for conversion to geothermal usages, and classed into four tiers. Only Tier 1 and Tier 2 well shapefiles were used in locating a region of interest for the case study. These oil and gas wells were assigned geothermal property ranges and tier ranks based on the interpretive maps of gradient and heat flow and not on intrinsic data from each well. Of the many wells assigned properties and mapped, Tier 1 wells accounted for the top 2% of wells with geothermal properties (heat flow and gradient) and had interpreted heat flows greater than 150 mW/m^2, with geothermal gradients greater than 70°C/km. Tier 2 wells accounted for the top 5% of wells with geothermal properties, and had interpreted heat flows between 120-150 mW/m^2, and geothermal gradients between 60-70°C/km.

The maps were all qualitatively analyzed, with three specific regions standing out from other areas. The first was Mount Princeton Hot Springs, near Buena Vista, Colorado, as this location has known and direct geothermal activity present, with the existence of hot springs, surface deformation and geothermal mineralogy (Figure 1). The second was near Boncarbo, Colorado, west of Trinidad, Colorado, which possessed indirect evidence of geothermal activity such as hot temperature-depth log recordings for certain exploratory wells, and high geothermal gradient and heat flow measurements (Figure 2a-2c). The third area was of original interest, in the San Luis Valley, because the valley is located directly on the Rio Grand rift. However, of the three sites, only the area around Trinidad was investigated in depth, because it possessed higher

geothermal potential according to CGS maps than the San Luis Valley, and the topography near Trinidad was less heterogeneous than the topography near Mount Princeton.

A Geographic Information System was generated, incorporating well point shapefiles used to make the three CGS maps used in qualitative visual analysis. This was combined with municipal polygon and polyline shapefiles to locate areas of interest. Projection and coordinate systems were altered to match the Universal Transverse Mercator (UTM) projection and datum used by the USGS for ASTER Level-1B imagery. Sorting was conducted on point shapefiles used to generate the Colorado Geological Survey Maps using Select by Attributes to generate an SQL query which only selected well points that were both Tier 1 and Tier 2 wells for both heat flow or gradient range. This was exported to a new shapefile that was used to locate regions of interest near Trinidad (Figure 3). As images were potentially difficult or costly to procure, the Trinidad region was selected for further analysis, but the San Luis Valley and Buena Vista regions were omitted.

Image Selection

The coordinates from specific well points near Trinidad were used to locate the general area for searching satellite imagery. Using the USGS EarthExplorer, ASTER Level-1B imagery was selected with footprint covering the location of interest. A polygon matching the footprint of selected imagery was drawn into ArcGIS® version 10.2 software to double check location of imagery in relation to the GIS data (Figure 3).

Image Pre-processing

The Trinidad imagery needed georeferencing and orthorectification against an input image generated through mosaicking several Digital Elevation Model (DEM) images of the

region. Six DEMs were mosaicked within ENVI version 5.2, and then used as input in orthorectification (Figure 4). As the DEM spatial resolution of 10 meters was more fine than the ASTER TIR imagery at 90 meters, the mosaicked DEM image was resampled to this coarser resolution using nearest neighbor resampling. Mosaicked DEM projection and resolution was matched to this thermal imagery, thus the output orthorectified thermal infrared ASTER image retained its native projection and resolution.

Qin's method for land surface temperature retrieval from Landsat ETM+ data utilized the Normal Differential Vegetation Index Thresholds Method ($NDVI^{THM}$) for emissivity calculation (Qin et al. 2011). This method provided a means of computing the emissivity of pixels classed as either vegetated, bare, or mixed, and a single-channel algorithm presented by Artis and Carnahan (1982) was applied (Qin et al. 2011). However, this method was less than ideal for ASTER thermal imagery, as ASTER has a higher spectral resolution than Landsat 7 ETM+, possessing five bands in the thermal infrared, versus Landsat ETM+ single thermal band (Table 1). Having five thermal channels allows for improved accuracy in land surface temperatures, because the five channels allow for iterative comparison using each of the five bands as a reference channel at least once. The more accurate algorithm for the ASTER data was the emissivity normalization algorithm (Kealy et al. 1993; Exelis Visual Information Solutions 2015). This algorithm calculates surface temperature in each of the five bands using a fixed emissivity value of 0.96. The highest temperature for each pixel is then used to calculate the more accurate emissivity values using the Planck function (Figure 5).

To do this, the algorithm first separates temperature from emissivity to calculate the temperature of each pixel in each of the five ASTER TIR bands. To calculate surface

temperature, a constant emissivity of 0.96 value is assumed so that an initial temperature calculation for each pixel in each of the five thermal channels can be generated. Each pixel then has five temperatures, and the highest temperature is assigned to that pixel as the pixel's temperature. This maximum temperature value is assumed to be the surface temperature and is then used to derive the land surface emissivity of each pixel within each of the five channels. This derived emissivity is then used to recalculate the emitted radiance for each band. The emitted radiance is then utilized to recalculate emissivities of each band and then these new emissivities are generated to recalculate radiance until a convergence threshold of emitted radiance is reached.

By using the emissivity normalization algorithm, pixels are given temperature values that will best represent the land surface temperature, based on the five band spectral resolution of ASTER. This is beneficial in locating thermal anomalous signatures because these signatures will be more easily located for quick screening to determine which anomalies are generated from subsurface thermal gradients, and which are the result of landcover emissivity. The emissivity normalization algorithm can aid in distinguishing between anomalies such as land covers that have lower albedos versus land covers with higher albedos. Land covers with higher thermal inertia can retain insolation for longer periods of time than other land surfaces (Atmospheric Correction, Exelis VIS). Once the algorithm was applied, an image was generated that possessed values for each pixel expressing temperature in Kelvin. Band Math within ENVI Classic was applied, converting temperature values from Kelvin to Celsius (Figure 6).

Image Processing and Threshold Calculation

Once the land surface temperature image was generated, and temperatures were in celsius, a threshold was selected to investigate the image for thermal anomalies. This was done qualitatively by looking at the image's histogram, indicating brightness values (Figure 7). Any anomalous thermal readings would likely reside within the farthermost tail of the histogram generated by the thermal image, and so various thresholds were chosen in ENVI Classic to create a binary mask. Using band math, any pixels that were less than a given temperature were given a value of zero, and anything greater than the threshold temperature was given a value of one. An initial boolean temperature mask generated 26,460 pixels with values between 21.39°C - 34.66°C (Figure 8). No finer mask could be produced in ENVI Classic, because only 21 pixels had temperatures greater than 30°C, a number too small for the software to classify. Setting the threshold to 30°C seemed appropriate, as this temperature represents the average geothermal gradient of 30°C/km of depth, where with one kilometer of depth, temperatures increase by 30°C. Because of this, temperatures greater than this could be considered above normal, and are often indicative of subsurface thermal gradient anomalies (Barbier 2000; van der Meer 2014). Although the count of pixels was low, possibly excluding some pixels having anomalously high temperatures, this method allowed a narrowing down to more specific regions of interest for analysis. For further classification, the image was moved into ArcGIS® version 10.2 software, where a final binary mask was produced, only retaining those pixels above 30°C.

Image Analysis

Within ArcMap™, Esri's basemap was used to qualitatively explore surfaces where anomalies were located with the intention of additional subsetting of the thermal ASTER image,

and for locating sites where ground truth spectroscopic field measurements could be conducted. Esri provides a satellite image basemap generated from DigitalGlobe at a spatial resolution of 0.3 meters (Figure 9). This image cannot be resampled to fit the coarse resolution of ASTER as it resides on a server provided by Esri. Overlay errors are thus present and unable to be altered without obtaining an image from DigitalGlobe of the region of interest for processing. The basemap appears to be shifted north and east, up one pixel, right one pixel, in comparison to the coarse $90m^2$ ASTER pixels. Qualitative observances of land cover can nonetheless be investigated using this basemap, to explore regions with possible anomalous readings.

Very few anomalous locations were found in the final compiled temperature image. Those discovered were explored using the high resolution basemap and by generating slope and aspect raster surfaces to determine if anomalous reads were located on sun facing slopes, or steep slopes (Figure 10 and 11). ArcGIS® Solar Radiation Tools were run on the image to determine what the sun angle was at the time the image was taken by the ASTER sensors. Solar radiation at the surface can be calculated for the atmospherically corrected image by multiplying the cosine of the Zenith angle by the insolation on a surface perpendicular to incoming solar radiation. The Zenith angle is dependent on longitude, latitude, and the sun's position in the sky at the time of *Terra's* passing when the ASTER image was obtained. A quantitative account of incoming solar radiation could then be removed to narrow down actual subsurface generated thermal anomalies. The image was too large for this analysis to be run adequately. The larger ASTER image would require further subsetting for these tools to work.

Results

Heat Map and Uncertainty

The Geothermal Heat Flow map used in selecting regions of interest was of an interpolated surface. As stated, the Colorado Geological Survey built the map using a least-squares best-fit linear interpolation calculation generated on point sources from several databases, supplemented with 40 temperature-depth logs derived from field research. As only 40 points were field-derived, only the data quality of these points were known as controlled by the CGS. All other point sources came from databases and field work from multiple sources of unknown methodological certainty. Having a wide variety of sources in data collection can introduce the possibility of measurement error in the dataset that is hard to quantify or mitigate. Each database or field collection could have been conducted using different standards for collection and metadata creation. However, as the maps were only used initially to locate a generalized region of interest, these possible inaccuracies do not play a factor in influencing the outcome of this study. Ideally, a field exploration of the discovered regions of interest would improve accuracy of the data and check the validity of the Heat Flow map surfaces used, but this was beyond the scope of the case study.

Purpose of Image Selection

The ASTER Level-1B registered radiance at the sensor product selected was from December 3, 2000, of a region near Trinidad, CO. Level-1B images are radiometrically calibrated and geometrically co-registered from the original Level-1A product. Applications of radiometric calibration and geometric correction coefficients were applied to the Level-1A imagery to produce the Level-1B image used; this accounts for atmospheric effects such as

scattering and atmospheric absorption. Atmospheric correction is beneficial for the initial exploratory analysis of geothermal resource potential, primarily because accounting for the atmosphere requires complex algorithms whose direct application are beyond the scope of this case study.

The image from 2000 was selected to avoid sensor malfunctions that began in early 2008. These led to an anomalous saturation of values in temperature detection, striping, and reduced location accuracy in the thermal and shortwave infrared wavelengths. As geothermal heat flow is likely to change very slowly over time, less current imagery would still provide adequate potential in finding anomalous thermal signatures.

Other images were explored, such as those covering Mount Princeton Hot Springs, but not selected for analysis. The topography near Mount Princeton was highly variable, encompassing multiple ecotones, including high plains desert to alpine ecosystems in a single image. This heterogenous topography would be difficult to quantify and remove in image analysis. Artifacts could be introduced that are resultant of a slope's aspect in relation to the sun, coupled with the highly variable land cover. Colorado's variable topography is a large challenge to the remotely sensed exploration of geothermal resources. For this reason, the Trinidad region was selected, as the landcover seemed more uniform in vegetation, and the topography less heterogenous in comparison to the region near Mount Princeton Hot Springs.

Pre-Processing Issues and the use of the Emissivity Normalization Algorithm

Orthorectification and georeferencing took more time than anticipated for the case study. This was made simpler after the generation of the mosaicked DEM, used to georeference the Level-1B thermal image. The original intention of the project was to follow the Qin *et al.*

methodology and conduct an NDVI as well as an emissivity calculation. However, as the imagery used was derived from *Terra's* ASTER sensor, five thermal bands were available, the Qin *et al* methodology was not the most efficient means. As Landsat ETM+ thermal band has only one thermal band, calculating NDVI was necessary to remove the effects of vegetation in thermal calculations via the vegetation fraction calculation (Qin et al. 2011). The Landsat ETM+ thermal band used a single-channel algorithm, which was not necessary for the emissivity normalization calculation used for the ASTER imagery. The five bands were compared to one another as reference channels as opposed to Landsat ETM+ single reference channel algorithm. This allowed for a more accurate measurement of temperature and emissivity, based on the explanation within the methods section. By selecting the highest temperature for each pixel in each of the five bands, the emissivity normalization calculation would capture any thermal anomalies present.

Threshold Calculation

A binary temperature mask was generated to locate anomalous pixels with higher temperature readings. Pixels below a given temperature were set to zero, those greater than a given temperature were set to one. The threshold calculation within ENVI Classic was only able to capture pixels that were 21°C or greater in temperature. This was because so few pixels existed within the image at these high temperatures. To compensate, the binary temperature mask was placed into ArcGIS® version 10.2 software and reclassified to only include pixels that had temperatures of 30°C or greater. This allowed for a more precise exploration of high anomalous surface temperatures that could be generated by subsurface geothermal activity.

Qualitative Exploration

Initial exploration of regional topographic effects in the ASTER Level-1B imagery used the ArcGIS® Solar Radiation Toolkit. These tools enable direct and diffuse insolation calculations down to specific hours within a day for a given region of interest. Tool use was attempted to obtain insolation information for the exact time the ASTER image was taken. The processing failed on several attempts, because the image was too large for the tools to be properly utilized.

Slope and aspect were calculated for the ASTER image. Observation suggested that most higher temperatures were the result of slopes with aspects facing the sun (Figures 11 and 12). The reclassified temperature mask representing pixels with temperatures greater than 30°C was overlaid on top of the slope and aspect layers to look for topographic effects. Slope and aspect were explored in regions of interest showing high thermal signatures (Figure 12a-b and Figure 13). A basemap was downloaded from Esri online, to note what landcover and topography looked like in high resolution imagery for regions of interest. Esri's basemap features 0.3m resolution imagery in the continental United States from DigitalGlobe. As pixel resolution of ASTER TIR imagery is 90 m^2, a discrepancy in resolution layering was present in the comparison. ASTER pixels overlaying the sub-meter resolution basemap were shifted South and East of where their center should have been (Figure 14 and Figure 15). This overlay problem was unfixable, as the sub-meter basemap imagery sits on Esri servers, and cannot be resampled to 90m^2 resolution.

It was expected thermal signatures would be hotter in a certain region of the image, based on the interpolated map surface and well temperature database measurements (Figure 2), but that

was not the case. Pixels displaying the highest temperatures were located in other areas, although some higher thermal temperatures did occur in areas near the well sites noted in the map (Figure 9). Here, a region where pixels with higher thermal signatures are present are located in close proximity to what appears to be an oil and gas exploratory site, or perhaps a wastewater pond for a hydraulic fracturing site (Figure 16). This higher temperature could be resulting from the land cover surfaces that have lower albedos that may also have greater thermal inertia, retaining heat for longer periods of time because of their darker tones.

Landcover with low albedo surfaces dark and black in color were often observed to be from coal mine tailings or coal deposits (Figure 14 and 16). The region captured in the ASTER image is known for its previous coal mining and oil and gas reserves. The coal is possibly skewing the thermal measurements captured by the emissivity normalization algorithm, being that it would retain heat for longer periods of time, be that heat generated from incoming solar radiation, or subsurface thermal anomalies. To account for this, field work involving mineral spectroscopy would be necessary for additional analysis. Although the landcover was darker in tone and likely possessed higher temperatures from the coal retaining heat, there were some unusual topographic deformations present that could be indicative of subsurface movement or geothermal activity (Figure 14). Lacking additional maps of faults, sinter cones, and calderas in the region and in the absence of field measurements, not enough data was present to determine if these topographic deformations present in the high-resolution imagery were from geothermal activity.

Conclusions and Discussion

Remote sensing is beneficial in improving geothermal reconnaissance methodologies and locating anomalies for furthering development of renewable energy technologies. The case study confirms issues noted in literature on geothermal reconnaissance using thermal infrared image analysis (Coolbaugh et al 2007). Temperatures with origins in subsurface geothermal activity are masked by the effects of insolation and its dialectic relationship with landcover. Land surfaces with lower albedos may also have a higher thermal inertia, and can retain heat from insolation for longer periods of time. However, a surface with higher thermal inertia will also retain subsurface heat longer. For this reason, additional investigation is needed into improving a geothermal reconnaissance methodology. Any additional analysis will require field measurements of surface deformation, mineralogy, thermal signatures, and other spectroscopic measurements that would confirm analysis conducted with satellite imagery.

For this study, it is likely that darker regions in the imagery where coal was present at the surface skewed thermal measurements obtained through the emissivity normalization algorithm. Accounting for this would require field analysis. Mineral spectroscopy would be beneficial in determining if the landcover is coal. Provided coal's unique spectral signature was known, these signatures could be accounted for and masked from the imagery. This can also be done by generating spectral indices using shortwave infrared imagery and remote sensing spectral signature processing techniques. Higher quality visible, shortwave infrared (SWIR) and hyperspectral imagery would provide further insight into the regions of interest initially discovered in this qualitative investigation, and could act as a second step in methodology after a thermal infrared exploration using ASTER. For example, DigitalGlobe's recent Worldview-3

platform has the capacity to SWIR imagery with 3.7m^2 native spatial resolution, commercially available at 9m^2 resolution. Imagery at this scale would allow for mineral mapping of specific regions of interest initially discovered using ASTER, but would provide a more in-depth reconnaissance into whether sites of interest possess minerals indicating presence of geothermal heat. Higher resolution thermal infrared analysis using unmanned aerial vehicles (UAVs) in the field fitted with thermal infrared and hyperspectral sensors could also improve analysis, because UAVs can take imagery at lower altitudes, thus reducing the scattering effects of the atmosphere. Having less atmosphere between sensor and ground could facilitate a more efficient methodology in locating subsurface geothermal anomalies, although it would introduce other issues, requiring geometric correction of arial platform movements.

Overlaying processing could be improved if high spatial resolution images, such as the basemap obtained from Esri online, were able to be reclassified. Purchasing sub-meter basemap imagery would allow for resampling, this coupled with field confirmation would improve analysis workflow. This would also allow a better comparison between images from different platforms with differing resolutions. Exelis ENVI version 5.3 has this overlaying feature built into their current software, and this automates both orthorectification and overlay processing. The use of ENVI version 5.3 would have improved efficiencies in time spent in understanding and properly applying orthorectification, allowing time to have been better spent in quantitative analysis of results.

Accounting for the effects of solar radiation topographically is essential to knowing whether anomalous thermal signatures are subsurface in origin. Masking out surfaces with low albedos, such as the coal, and slopes facing the sun could be done prior to emissivity

normalization. Subsetting larger images to smaller regions of interest where anomalous signatures were discovered could allow for the application of the ArcGIS® Solar Radiation Tools. Further comparison with evening imagery would be beneficial. No evening imagery was present for the ASTER imagery used, which is why this was not conducted. Evening imagery is preferred for thermal infrared analysis, because it immediately reduces the impact of insolation (Coolbaugh et al 2007). Monitoring diurnal effects and thermal inertia across a longer time period would also streamline a methodology. By measuring a region of interest through yearly or seasonal comparison, thermal inertia of certain surfaces could be quantified, allowing for a clearer understanding of anomalous temperature origins.

The Trinidad region is experiencing dramatic change with increased oil and gas development incorporating hydraulic fracturing methods (Berkman and Morgan 2010; Sares 2009). It is unknown how oil and gas development in this region will impact geothermal resource potential, or how hydraulic fracturing activity will influence thermal signatures that can be monitored using thermal infrared imagery. Monitoring development through satellite image analysis to quantify changes and possible influences oil and gas extraction has on geothermal resources in the Trinidad region could prove helpful in understanding the impacts of hydraulic fracturing. Monitoring changes in this region could also improve geothermal reconnaissance for the development of Enhanced Geothermal Systems (EGS) in the area, a type of geothermal energy that utilizes the methods developed through hydraulic fracturing exploration, but to generate electricity with zero-direct greenhouse gas emissions (Goldstein et al. 2011).

This investigation echoes the work of van der Meer *et al* : further work is needed to create an efficient geothermal reconnaissance workflow that is reproducible and has long-term

monitoring capabilities of surface and subsurface geothermal features (2014). A future expansion of this initial workflow is a goal, through incorporating thermal analysis, *in situ* surface spectrometry, and mineral mapping involving hyperspectral and high resolution shortwave infrared sensors is suggested to improve on this qualitative analysis. Field monitoring using UAVs fitted with thermal infrared sensors is of interest to build a dataset of higher spatial resolution in the thermal infrared wavelengths, and to monitor regions with geothermal potential over time. Regions in Colorado with geothermal potential, such as the Trinidad region and the San Luis Valley, could be used to further an adaptive remote sensing workflow incorporating GIS data gathered in the field with satellite and areal platform imagery. Another requisite in improving this workflow is to account for insolation in relation to the topographic effects of slope and aspect, and land cover thermal inertia. Improved understanding of landcover spectroscopy is essential, looking for example, for impacts of geothermal heat flux on vegetation health, soil geochemistry and soil moisture in the region. Masking out, classifying and quantifying these effects would help to rule out anomalous temperatures that are not geothermal, and locate temperatures that are.

Acknowledgments

This project was made possible with funding from the von Dreden Stacey Fellowship through the University of Colorado Department of Geography. Guidance from members of the Earth Sciences Observation Center (ESOC) within the Cooperative Institute for Research in Environmental Sciences (CIRES) directed by Dr. Waleed Abdalati was vital. Assistance and guidance provided by Dr. Khalid Hussein on project methodological development was indispensable in the development of this project. Advice from Michael MacFerrin, PhD student of Geography in the fledgling stages of this thesis benefitted this project's development and were appreciated. Editing in final imagery and technical writing benefitted from input by Beth Billington. Superb administration of organizing defense schedule would not have been made possible without the support of Lornay Hansen.

Bibliography

2014 Renewable Energy Data Book. 1st ed. US Department of Energy, 2014. Web. 9 Nov. 2015.

Arnórsson, Stefán, Jón Örn Bjarnason, N. Giroud, Ingvi Gunnarsson, and A. Stefánsson. "Sampling and analysis of geothermal fluids." *Geofluids* 6, no. 3 (2006): 203-216.

Artis, David A., and Walter H. Carnahan. "Survey of emissivity variability in thermography of urban areas." *Remote Sensing of Environment* 12, no. 4 (1982): 313-329.

"Atmospheric Correction," Exelis Visual Information Solutions, Boulder, Colorado, accessed October 11, 2015, http://www.exelisvis.com/docs/AtmosphericCorrection.html#references.

Barbier, Enrico. "Geothermal energy technology and current status: an overview." *Renewable and Sustainable Energy Reviews* 6, no. 1 (2002): 3-65.

Bateson, Luke, M. Vellico, S. E. Beaubien, J. M. Pearce, A. Annunziatellis, G. Ciotoli, F. Coren, S. Lombardi, and Stuart Marsh. "The application of remote-sensing techniques to monitor CO 2-storage sites for surface leakage: method development and testing at Latera (Italy) where naturally produced CO 2 is leaking to the atmosphere." *International Journal of Greenhouse Gas Control* 2, no. 3 (2008): 388-400.

Berkman, Frederick E., Christopher J. Carroll, Nicholas A. Watterson. "Interpretive Geothermal Heat Flow Map of Colorado" [map on optical data file]. First Edition. ca. 1:500,000. Map Series 45, Plate 1; Denver, CO: Colorado Geological Survey, Department of Natural Resources, July 2008.

Berkman, Frederick E., Paul Morgan, Nicholas A. Watterson. "Oil and Gas Wells in Areas of Colorado with Superior Geothermal Properties" [map on optical data file]. First Edition. ca. 1:500,000. Denver, CO: Colorado Geological Survey, Department of Natural Resources, March 2010.

Berkman, Frederick E., Nicholas A. Watterson. "Interpretive Geothermal Gradient Map" [map on optical data file]. First Edition. ca. 1:500,000. Denver, CO: Colorado Geological Survey, Department of Natural Resources, March 2010.

Carnec, Claudie, and Hubert Fabriol. "Monitoring and modeling land subsidence at the Cerro Prieto geothermal field, Baja California, Mexico, using SAR interferometry." Geophysical Research Letters 26, no. 9 (1999): 1211-1214.

Carranza, Emmanuel John M., F. J. A. Van Ruitenbeek, C. Hecker, Mark van der Meijde, and Freek D. van der Meer. "Knowledge-guided data-driven evidential belief modeling of

mineral prospectivity in Cabo de Gata, SE Spain." *International Journal of Applied Earth Observation and Geoinformation* 10, no. 3 (2008a): 374-387.

Carranza, Emmanuel John M., Hendro Wibowo, Sally D. Barritt, and Prihadi Sumintadireja. "Spatial data analysis and integration for regional-scale geothermal potential mapping, West Java, Indonesia." *Geothermics* 37, no. 3 (2008b): 267-299.

Chronic, Halka, and Felicie Williams. *Roadside geology of Colorado*. Mountain Press, 2002, p. 75-80, 180-184.

Choate, Raoul, and Craig T. Rightmire. "Influence of the San Juan Mountain geothermal anomaly and other Tertiary igneous events on the coalbed methane potential in the Piceance, San Juan, and Raton Basins, Colorado and New Mexico." In *SPE Unconventional Gas Recovery Symposium*. Society of Petroleum Engineers, 1982.

Chung, C. F., and F. P. Agterberg. "Regression models for estimating mineral resources from geological map data." *Journal of the International Association for Mathematical Geology* 12, no. 5 (1980): 473-488.

Coolbaugh, M. F., R. E. Zehner, G. L. Raines, G. L. Oppliger, and C. Kreemer. "Regional prediction of geothermal systems in the Great Basin, USA using weights of evidence and logistic regression in a Geographic Information System (GIS)." In *International Association of Mathematical Geology Annual Conference Proceedings, Toronto, Canada*, pp. 505-510. 2005.

Coolbaugh, M. F., C. Kratt, A. Fallacaro, W. M. Calvin, and J. V. Taranik. "Detection of geothermal anomalies using advanced spaceborne thermal emission and reflection radiometer (ASTER) thermal infrared images at Bradys Hot Springs, Nevada, USA." *Remote Sensing of Environment* 106, no. 3 (2007): 350-359.

Crosta, A. P., C. R. De Souza Filho, F. Azevedo, and C. Brodie. "Targeting key alteration minerals in epithermal deposits in Patagonia, Argentina, using ASTER imagery and principal component analysis." *International Journal of Remote Sensing* 24, no. 21 (2003): 4233-4240.

Gao, Wei, Stephen P. Grand, W. Scott Baldridge, David Wilson, Michael West, James F. Ni, and Richard Aster. "Upper mantle convection beneath the central Rio Grande rift imaged by P and S wave tomography." *Journal of Geophysical Research: Solid Earth (1978–2012)* 109, no. B3 (2004).

Goldstein, B., et al. “Geothermal Energy: Special Report on Renewable Energy Sources and Climate Change Mitigation.” Cambridge University Press, Cambridge, United Kingdom and New York, NY, USA, 2011.

Haselwimmer, Christian, and Anupma Prakash. "Thermal infrared remote sensing of geothermal systems." In *Thermal Infrared Remote Sensing*, pp. 453-473. Springer Netherlands, 2013.

Hook, Simon J., Andrew R. Gabell, Andrew A. Green, and Peter S. Kealy. "A comparison of techniques for extracting emissivity information from thermal infrared data for geologic studies." *Remote Sensing of Environment* 42, no. 2 (1992): 123-135.

Huntington, Jonathan F. "The role of remote sensing in finding hydrothermal mineral deposits on Earth." In Ciba Foundation Symposium 202-Evolution of Hydrothermal Ecosystems on Earth (And Mars?), pp. 214-235. John Wiley & Sons, Ltd., 1996.

Kealy, Peter S., and Simon J. Hook. "Separating temperature and emissivity in thermal infrared multispectral scanner data: Implications for recovering land surface temperatures." *Geoscience and Remote Sensing, IEEE Transactions on* 31, no. 6 (1993): 1155-1164.

Kristmannsdóttir, Hrefna, and Halldór Ármannsson. "Environmental aspects of geothermal energy utilization." *Geothermics* 32, no. 4 (2003): 451-461.

Kruse, Fred A. "Mapping surface mineralogy using imaging spectrometry." *Geomorphology* 137, no. 1 (2012): 41-56.

Majer, Ernest L., Roy Baria, Mitch Stark, Stephen Oates, Julian Bommer, Bill Smith, and Hiroshi Asanuma. "Induced seismicity associated with enhanced geothermal systems." *Geothermics* 36, no. 3 (2007): 185-222.

Nash, Gregory D., Joseph N. Moore, and Todd Sperry. "Vegetal-spectral anomaly detection at the Cove Fort-Sulphurdale thermal anomaly, Utah, USA: implications for use in geothermal exploration." *Geothermics* 32, no. 2 (2003): 109-130.

Noomen, M. F., and A. K. Skidmore. "The effects of high soil CO2 concentrations on leaf reflectance of maize plants." *International Journal of Remote Sensing* 30, no. 2 (2009): 481-497.

Noorollahi, Younes, Ryuichi Itoi, Hikari Fujii, and Toshiaki Tanaka. "GIS integration model for geothermal exploration and well siting." *Geothermics* 37, no. 2 (2008): 107-131.

Qin, Qiming, Ning Zhang, Peng Nan, and Leilei Chai. "Geothermal area detection using Landsat ETM+ thermal infrared data and its mechanistic analysis—A case study in Tengchong, China." *International Journal of Applied Earth Observation and Geoinformation* 13, no. 4 (2011): 552-559.

Rogan, John, and DongMei Chen. "Remote sensing technology for mapping and monitoring land-cover and land-use change." *Progress in Planning* 61, no. 4 (2004): 301-325.

Sares, Matthew A., Paul Morgan, and V. J. Grauch. "Geothermal Resources of Colorado and the Potential for Electrical Power Generation." *Search and Discovery* 30 (2009).

Tank, Volker, Hardy Pfanz, and Hermann Kick. "New remote sensing techniques for the detection and quantification of earth surface CO 2 degassing." J*ournal of Volcanology and Geothermal Research* 177, no. 2 (2008): 515-524.

van der Meer, Freek D., Harald MA Van der Werff, Frank JA van Ruitenbeek, Chris A. Hecker, Wim H. Bakker, Marleen F. Noomen, Mark van der Meijde, E. John M. Carranza, J. Boudewijn de Smeth, and Tsehaie Woldai. "Multi-and hyperspectral geologic remote sensing: A review." *International Journal of Applied Earth Observation and Geoinformation* 14, no. 1 (2012): 112-128.

van der Meer, Freek, Christoph Hecker, Frank van Ruitenbeek, Harald van der Werff, Charlotte de Wijkerslooth, and Carolina Wechsler. "Geologic remote sensing for geothermal exploration: A review." *International Journal of Applied Earth Observation and Geoinformation* 33 (2014): 255-269.

Vaughan, R. Greg, Laszlo P. Keszthelyi, Jacob B. Lowenstern, Cheryl Jaworowski, and Henry Heasler. "Use of ASTER and MODIS thermal infrared data to quantify heat flow and hydrothermal change at Yellowstone National Park." *Journal of Volcanology and Geothermal Research* 233 (2012): 72-89.

Wilson, David, Richard Aster, Michael West, James Ni, Steve Grand, Wei Gao, W. Scott Baldridge, Steve Semken, and Paresh Patel. "Lithospheric structure of the Rio Grande rift." *Nature* 433, no. 7028 (2005): 851-855.

Ziagos, John, Benjamin R. Phillips, Lauren Boyd, Allan Jelacic, Greg Stillman, and Eric Hass. "A technology roadmap for strategic development of enhanced geothermal systems." In *Proceedings of the 38th Workshop on Geothermal Reservoir Engineering, Stanford, CA*, pp. 11-13. 2013.

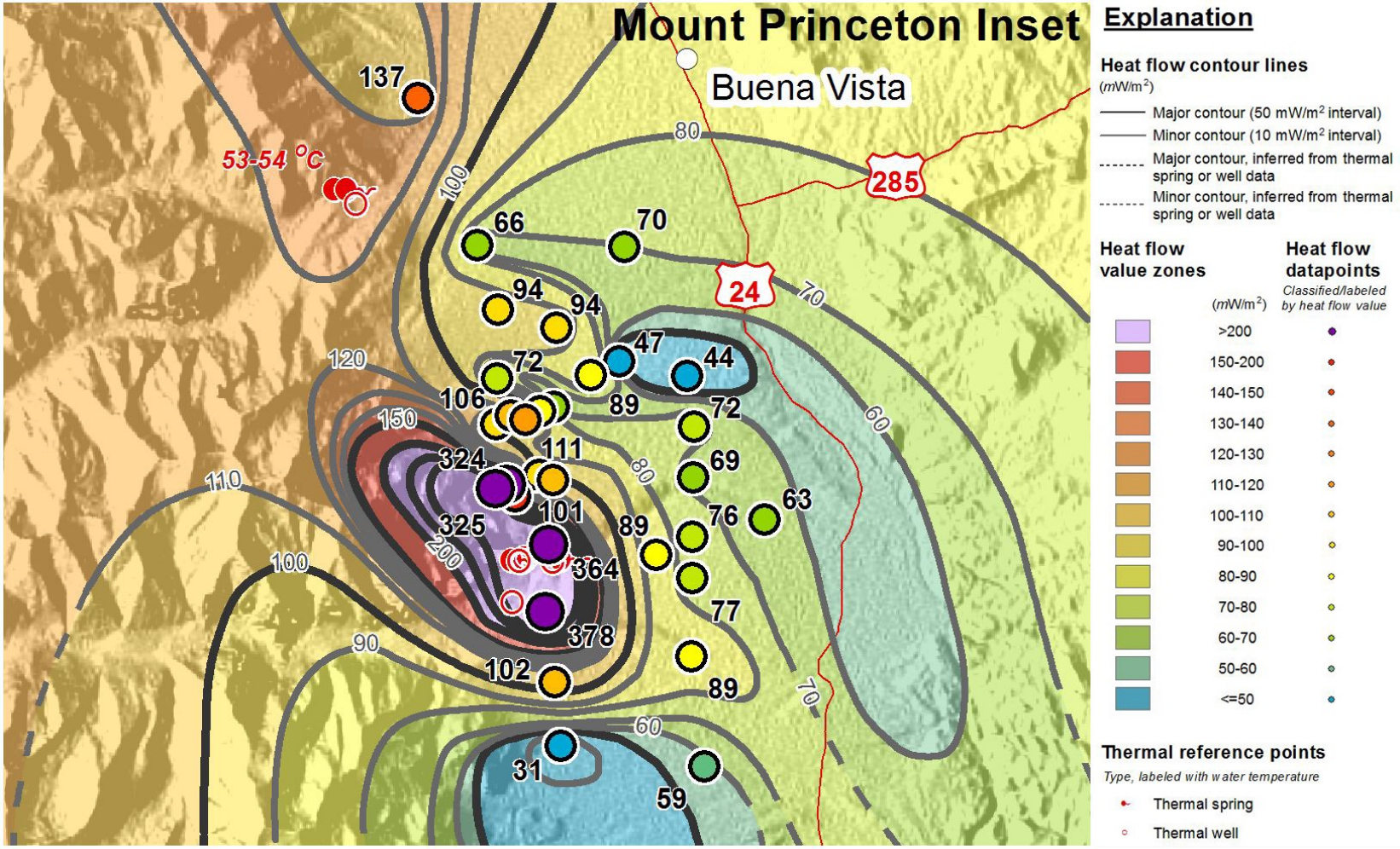

Figure 1.
Inset map from the "Interpretive Geothermal Heat Flow Map of Colorado," showing geothermal activity around Mount Princeton Hot Springs, near Buena Vista, CO.

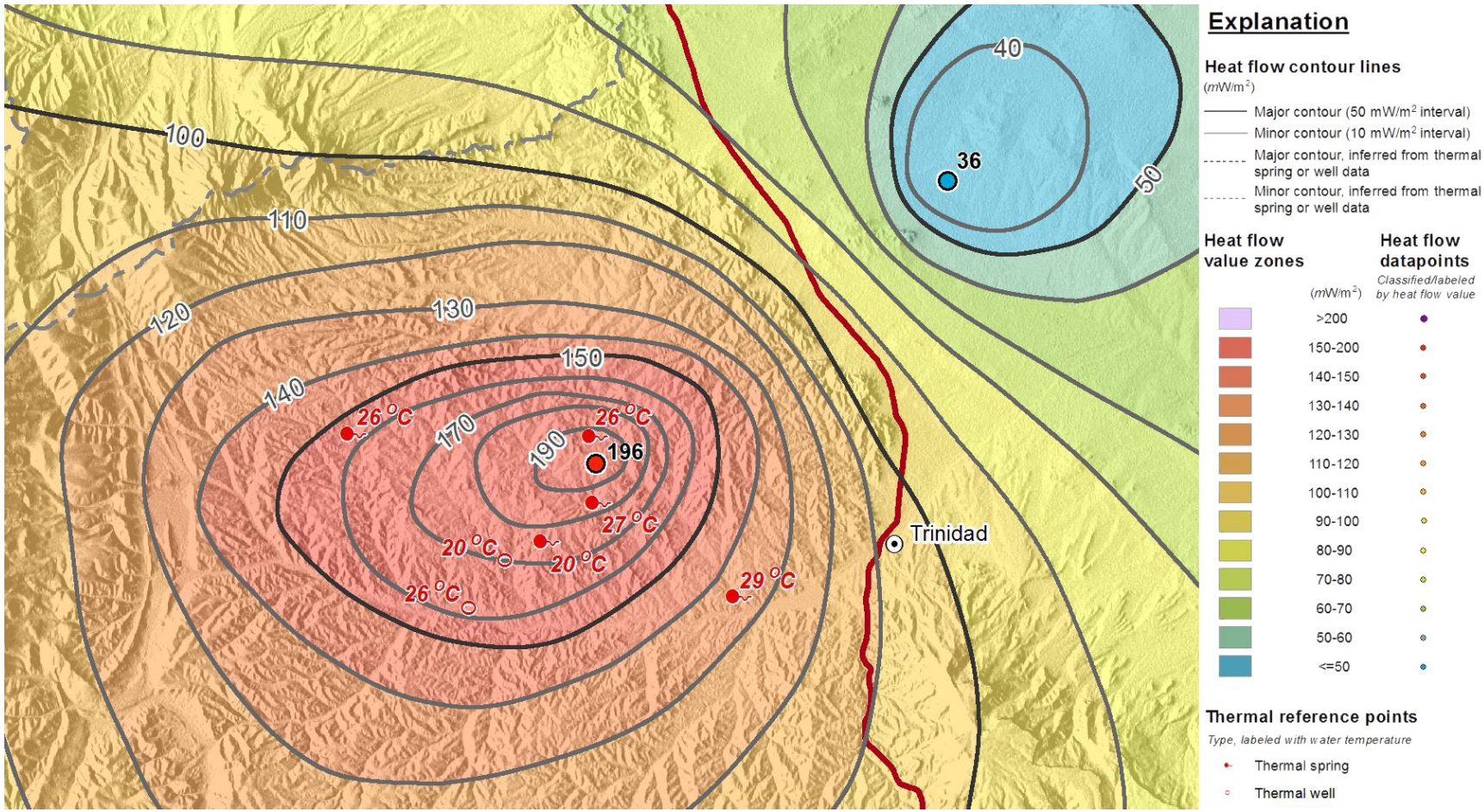

Figure 2a.

Inset near Trinidad, CO from the "Interpretive Geothermal Heat Flow Map of Colorado," showing geothermal activity around near Boncarbo, CO possessing high geothermal heat flow measurements. Geothermal heat flow is calculated for each well by multiplying composite rock thermal conductivity by geothermal gradient for a given area. Geothermal heat flow is commonly displayed in units of milliWatts per square meter (mW/m^2).

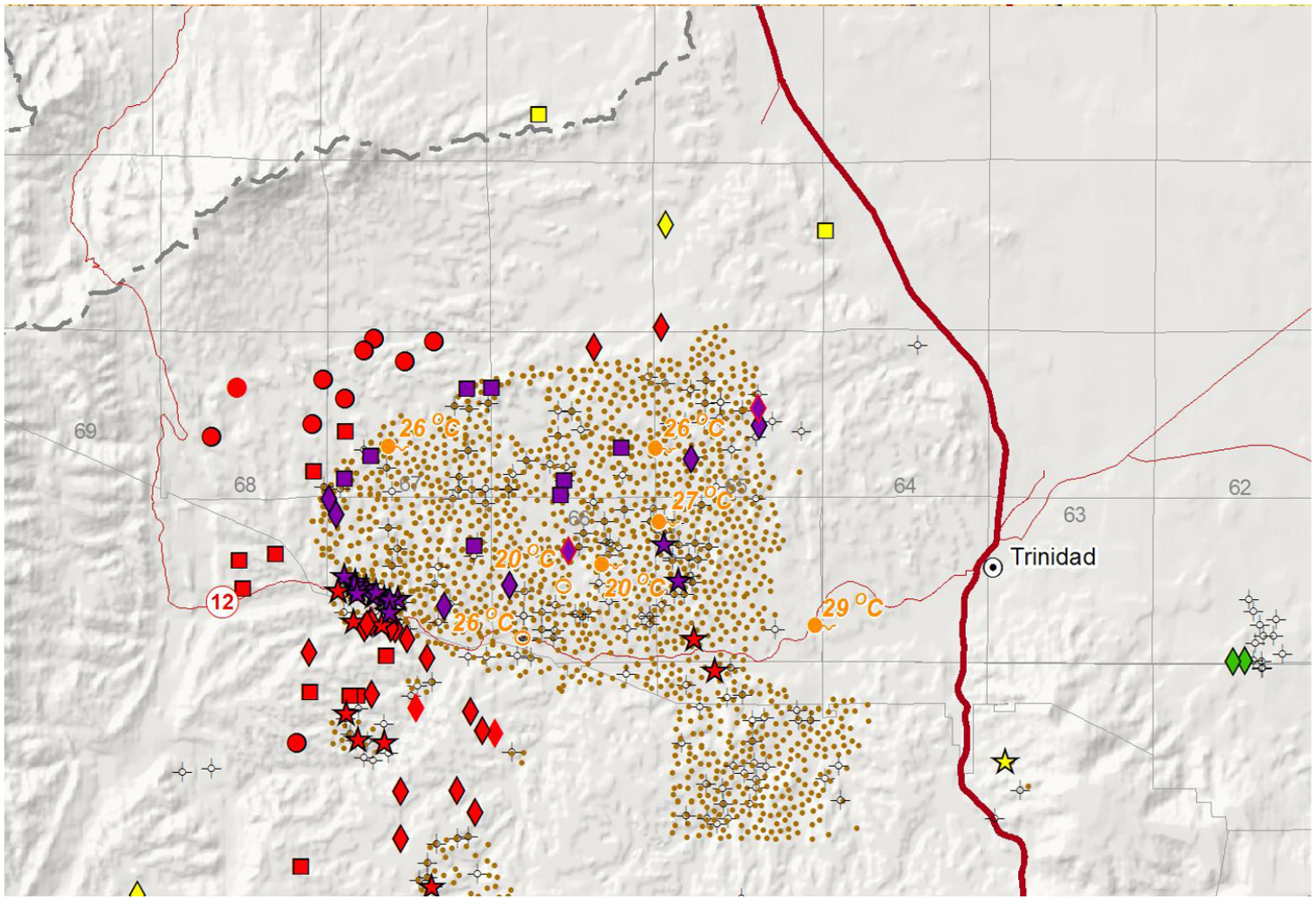

Figure 2b.
Inset from the "Oil and Gas Wells in Areas of Colorado with Superior Geothermal Properties" showing prospective wells with high geothermal potential around Trinidad, CO.

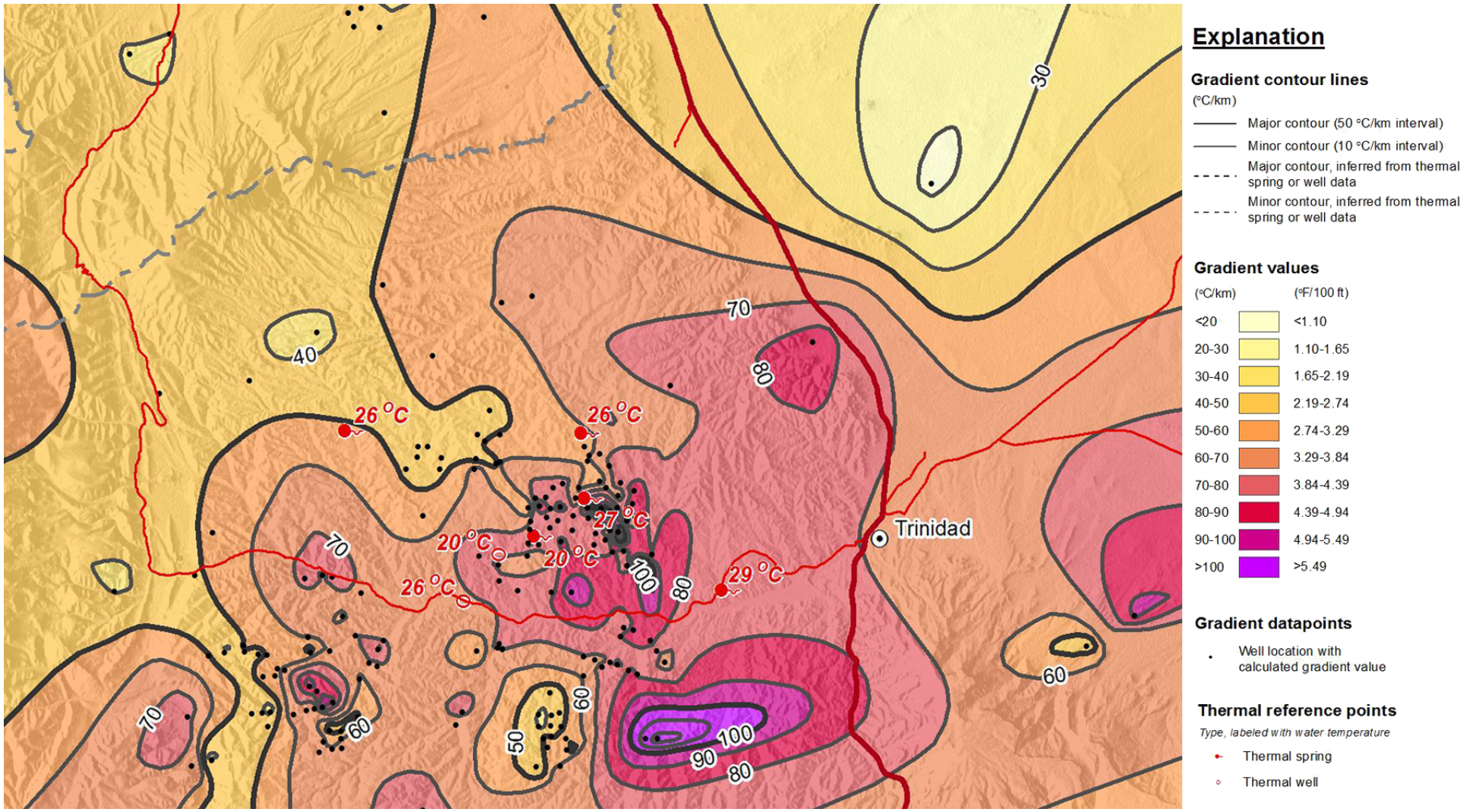

Figure 2c.

Inset from the "Interpretive Geothermal Gradient Map of Colorado," showing the geothermal gradient with field datapoints around Trinidad, CO. Geothermal gradient is the change in temperature over distance, expressed in units of degrees Celsius per kilometer (°C/km). It is a proxy for quantifying depth- temperature relationship in evaluating geothermal resource potential. Distance is the depth into the Earth given by a borehole or well.

Figure 3.
Selected image footprint and Tier 1 and 2 wells near Trinidad, CO. Tier 1 wells are the top ~2% of wells for each of the geothermal properties (gradient and heat flow), Tier 2 wells represent the top ~5% for both gradient and heat flow. An SQL query was run to only include wells that were both Tier 1 and Tier 2 in either thermal gradient or heat flow.

Mosaicked Digital Elevation Models for Image Analysis

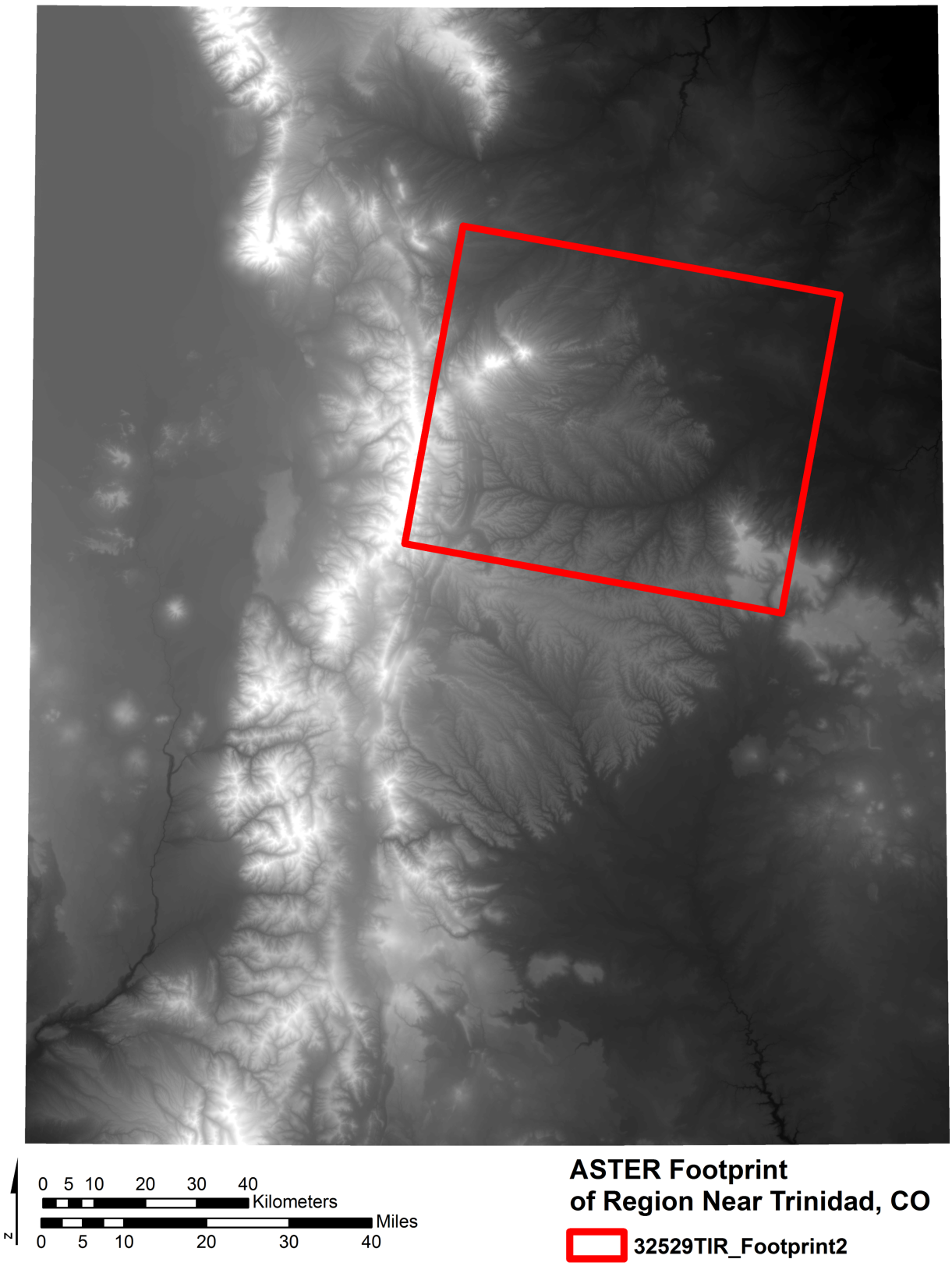

Figure 4.
Six $10m^2$ spatial resolution Digital Elevation Models (DEMs) were mosaicked together to obtain elevation for the selected ASTER TIR image. The final product was clipped to fit the ASTER footprint, and resampled to $90m^2$ to match the thermal image resolution.

Table 1. Thermal Sensor Spatial, Spectral, and Temporal Resolutions

Platform	Number of Bands covering Thermal Infrared	TIR Band Spatial Resolution	TIR Band Spectral Resolution (µm)	TIR Band Temporal Resolution
Landsat 7 ETM+	**1**	**60m2**	**Band 6: 10.31-12.36**	**16 Days**
Landsat 8 TIRS	**2**	**100m2**	**Band 10-11: 10.60-12.51**	**16 Days**
***Terra* ASTER**	**5**	**90m2**	**Bands 10-14: 8.125 - 11.65**	**16 Days**

$$L(\lambda) = \left(\frac{2hc^2}{\lambda^5}\right)\left(\frac{1}{e^{ch/\lambda kT}-1}\right)$$

Figure 5.
The Planck Function. Energy (Joules) emitted per second per unit wavelength per steradian from one square meter of a perfect blackbody at temperature. This is used when calculating the emissivity normalization, generating temperatures and emissivities for each pixel.

T = Temperature of the blackbody
h = Planck's constant (6.63×10^{-34} Js)
c = Speed of Light (3.00×10^{8} m/s)
λ = wavelength
k = Boltzmann's constant (1.38×10^{-23} J/K)

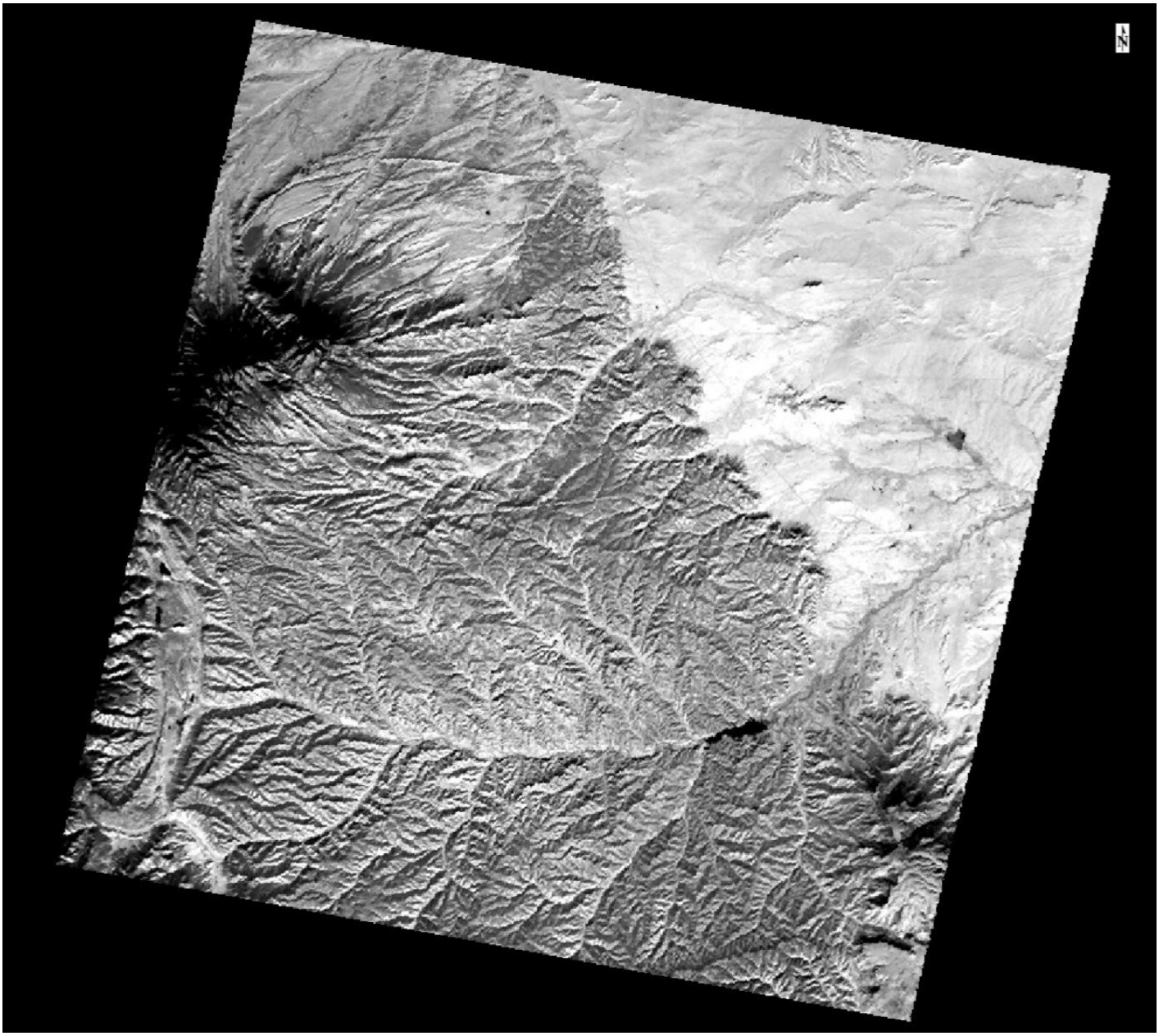

Figure 6.
ASTER Thermal image generated with the emissivity normalization algorithm. Brightness values of each pixel correspond to the highest temperature of all five ASTER TIR bands, altered from Kelvin to Celsius.

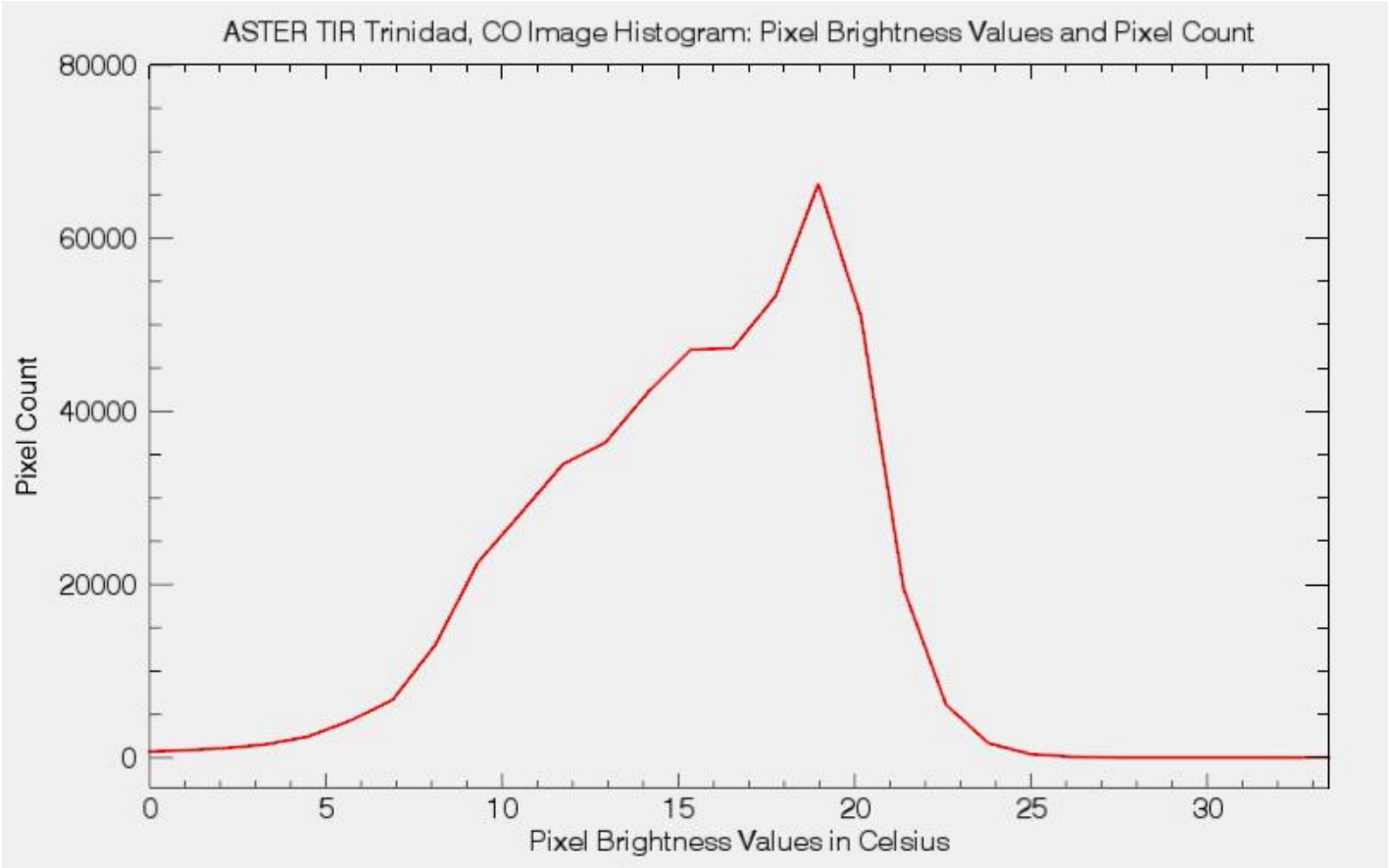

Figure 7.
Histogram depicting total pixels within the ASTER TIR image generated with the emissivity normalization algorithm (Figure 6). The histogram was used to select pixels above ~21°C.

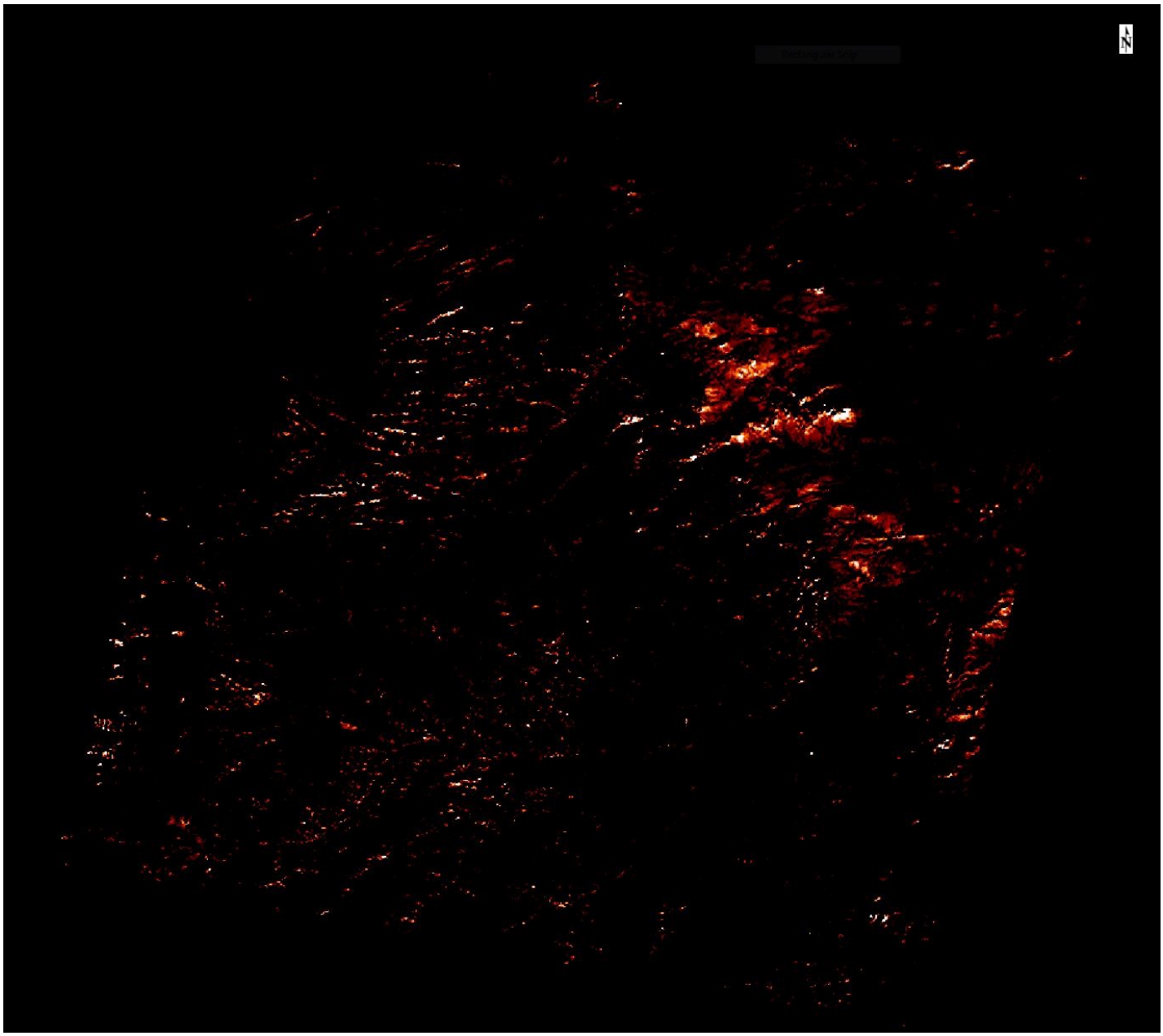

Figure 8.
Boolean temperature mask of the Trinidad, CO region. Pixels in red are between 21.39°C - 34.66°C. This image was generated within ENVI, and further classified within ArcMap™. These pixels could represent regions where possible subsurface thermal anomalies are present. Regions possessing the highest temperatures were further investigated.

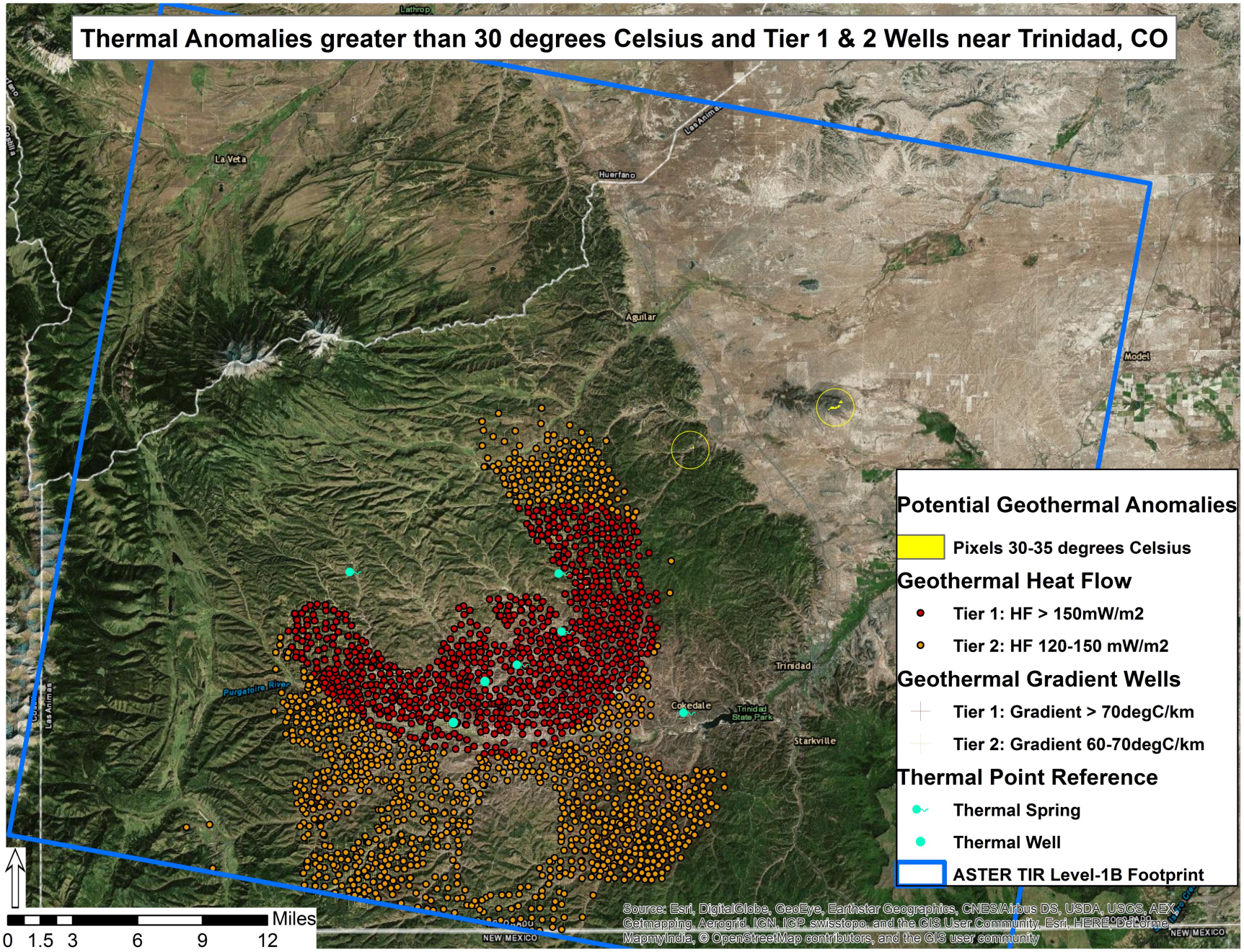

Figure 9.
High resolution basemap revealing topography of the Trinidad, CO region where potential thermal anomalies were found. Pixels with temperatures between 30°C - 34.66°C are in yellow. Tier 1 and Tier 2 wells possessing high thermal gradient and heat flows are also located in the imagery. The highest temperature pixels were not located in the anticipated region around the wells.

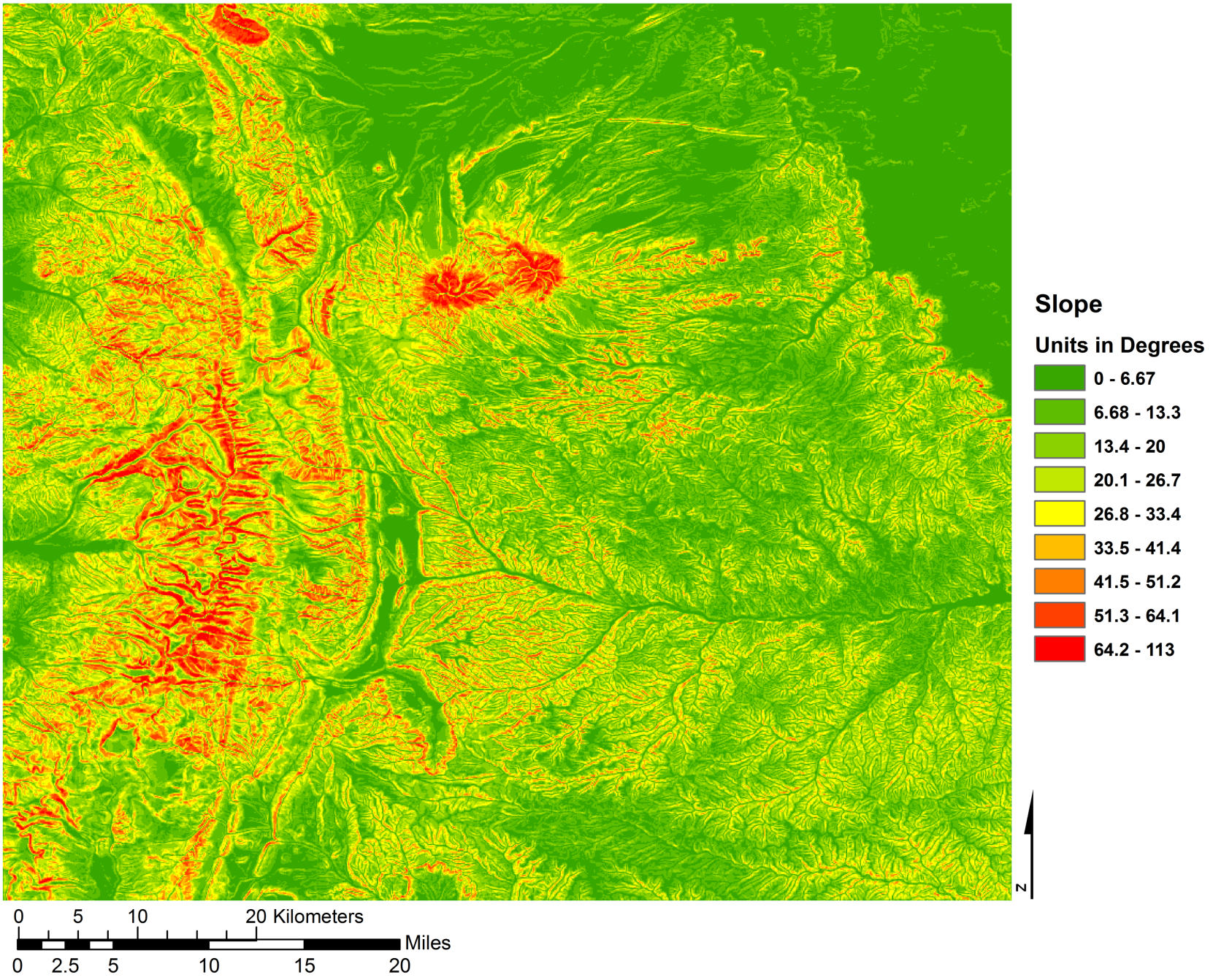

Figure 10.
Slope of the region of interest. This image was used to determine if anomalous regions were located on steeper slopes that faced the sun. Accounting for insolation and surface thermal inertia helps in finding subsurface geothermal anomalies.

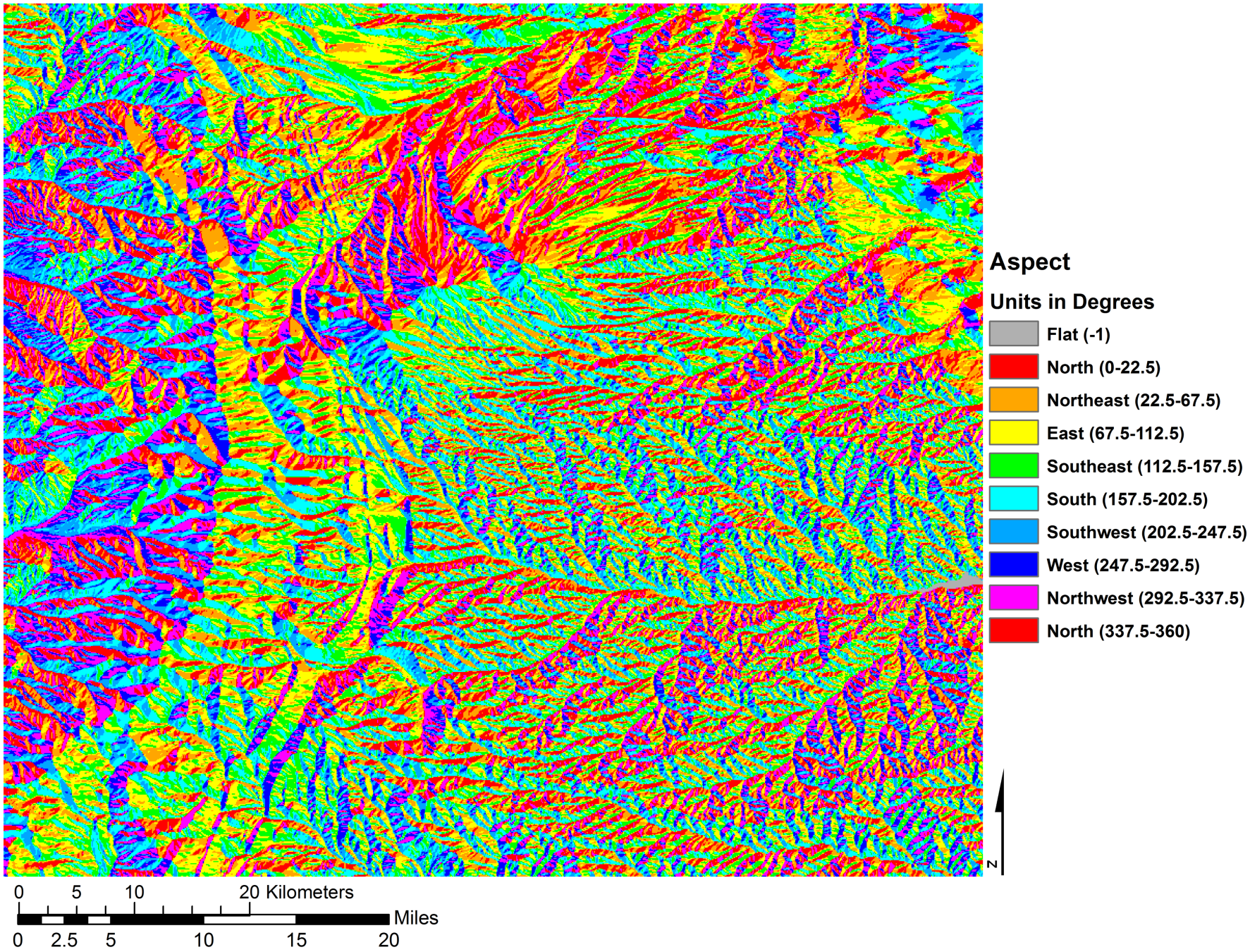

Figure 11.

Aspect of the region of interest. This image was used to determine if pixels displaying anomalous temperatures were located in areas facing the sun. Like Figure 10, this image was used to explore methods of removing effects of the sun, and to account for thermal inertia.

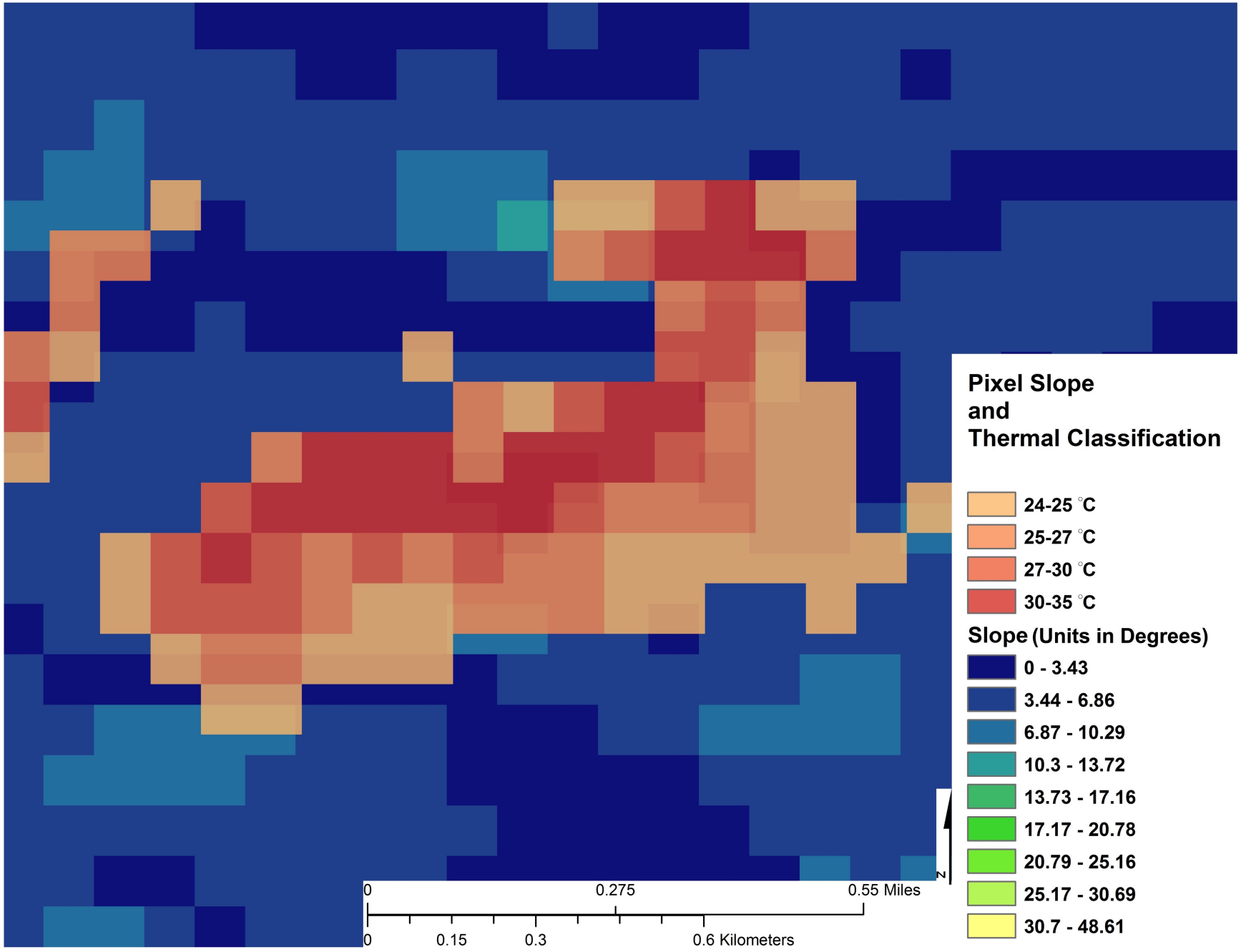

Figure 12a. Anomalous Region 1

Overlay of anomalous region with slope measurements. This region included pixels with the highest temperatures found in the ASTER TIR image. Slope pixels (in blue) have steeper slopes if colors are lighter, and are more flat in slope if colors are darker blue.

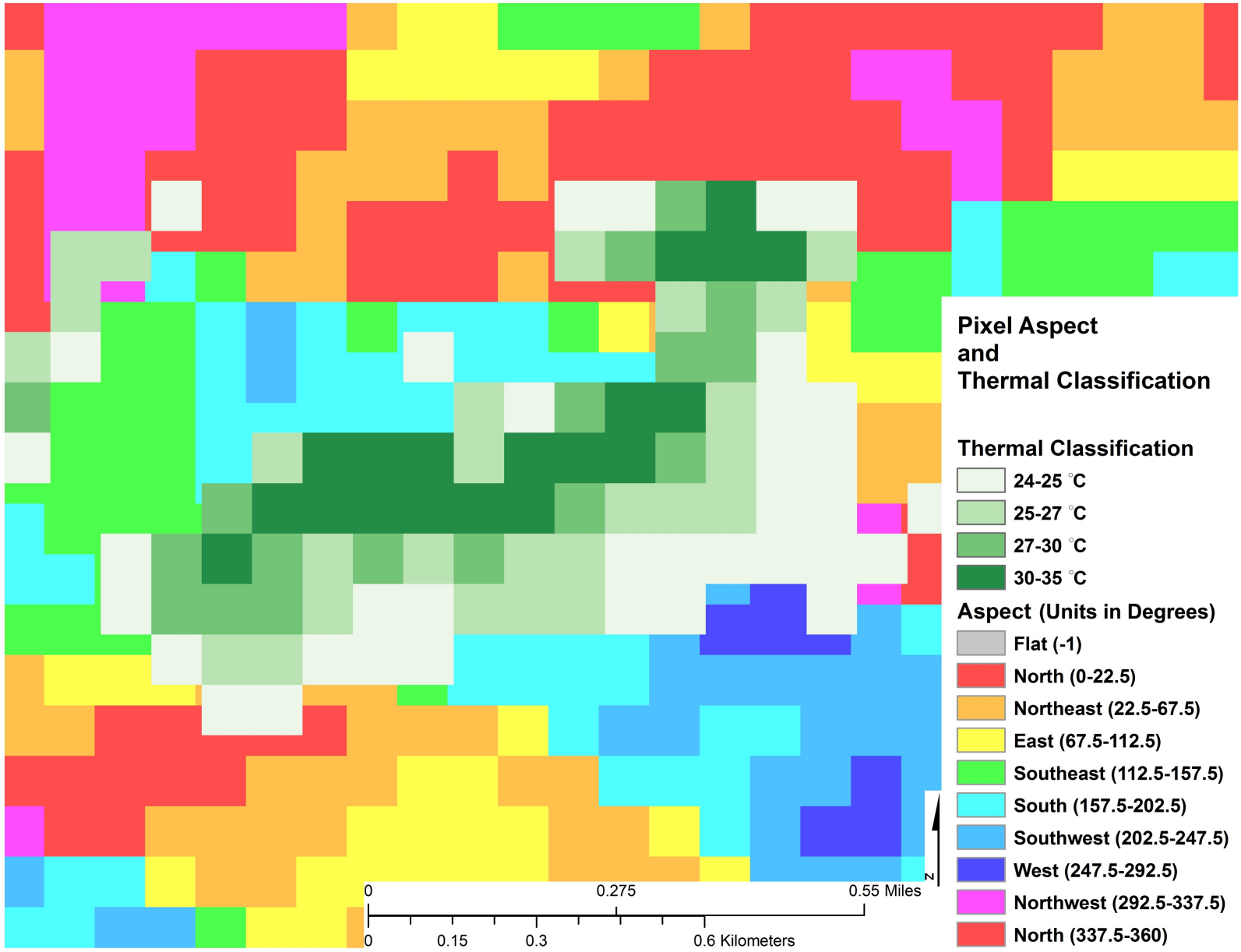

Figure 12b. Anomalous Region 1

Overlay of anomalous region (in forest green) with aspect measurements. This region included pixels with the highest temperatures found in the ASTER TIR image. Aspect pixels (in background) have slopes facing a particular direction. This is used to gauge if the slope was facing the sun throughout the day, to account for diurnal insolation.

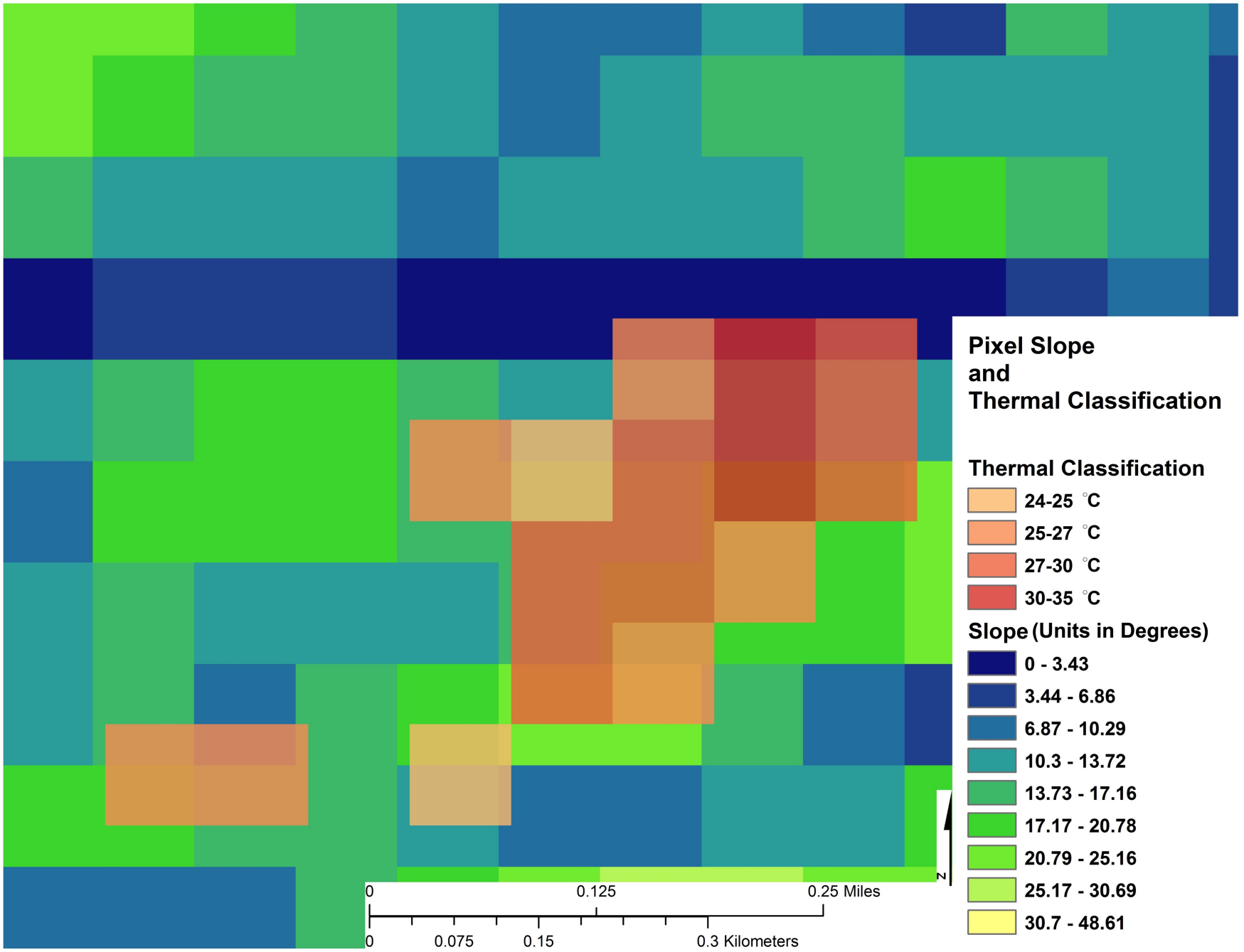

Figure 13a. Anomalous Region 2

Overlay of second anomalous region (in orange) with slope measurements. This region included pixels with the higher temperatures found in the ASTER TIR image. Slope pixels (in background) have steeper slopes if their colors are brighter (trending toward yellow).

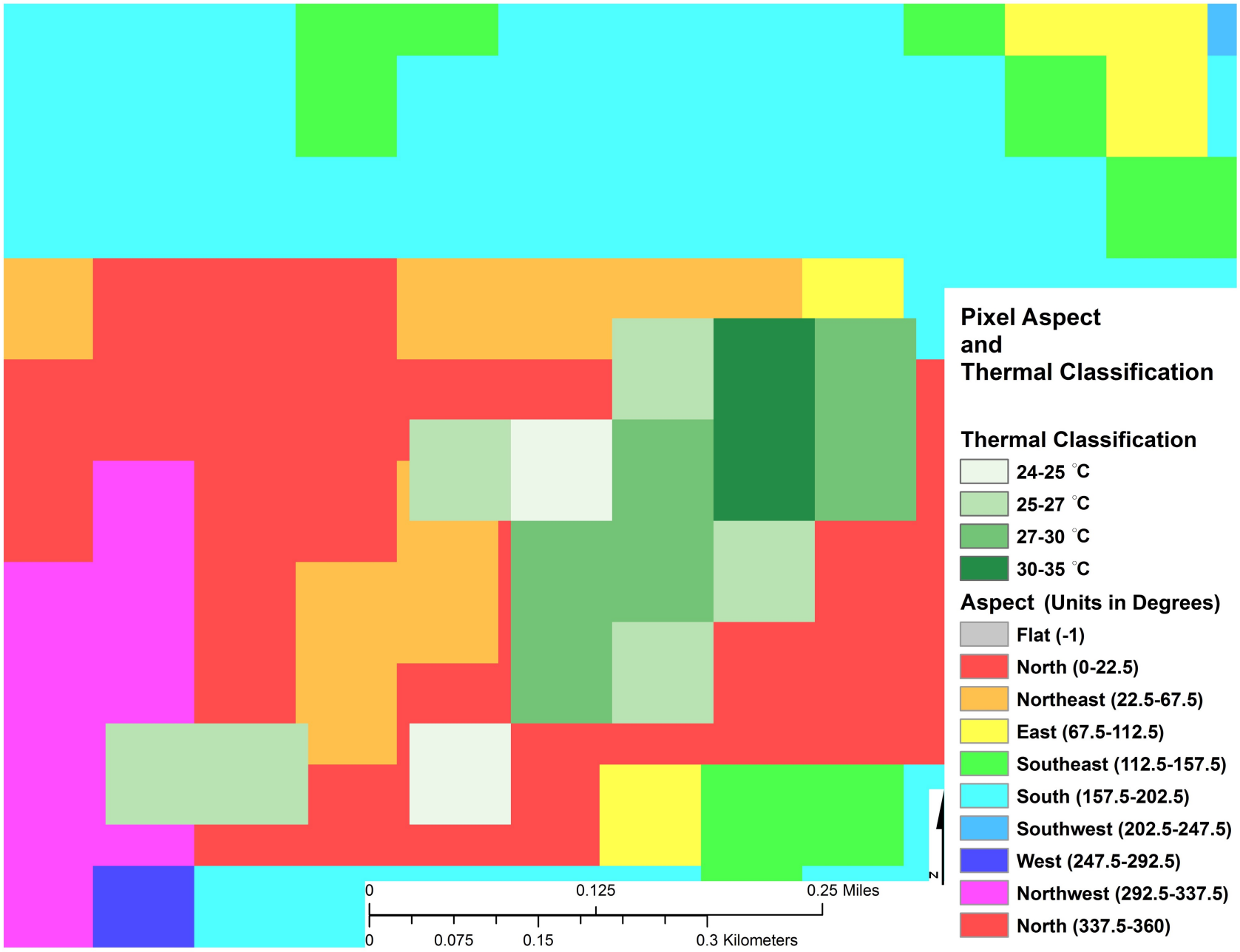

Figure 13b. Anomalous Region 2

Overlay of anomalous region (in forest green) with aspect measurements. This region included pixels with the higher temperatures found in the ASTER TIR image. Aspect pixels (in background) have slopes facing a particular direction. This is used to gauge if the slope was facing the sun throughout the day, to account for diurnal insolation.

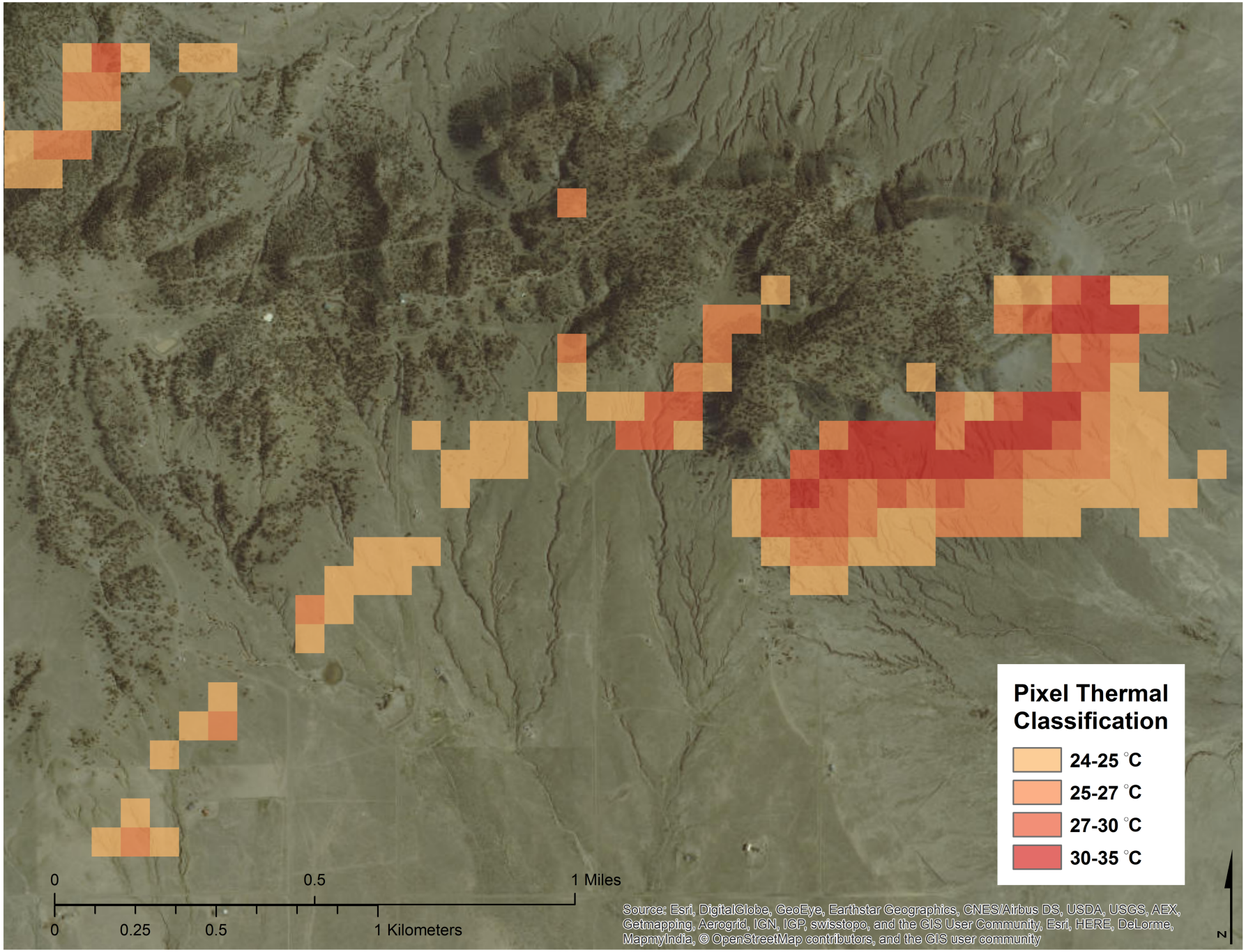

Figure 14. Anomalous Region 1

Overlay of anomalous pixels and high resolution basemap. The topography may indicate presence of faulting that could indicate anomalies come from subsurface geothermal energy. Further *in situ* spectroscopic analysis is required to better understand the geologic processes of this location.

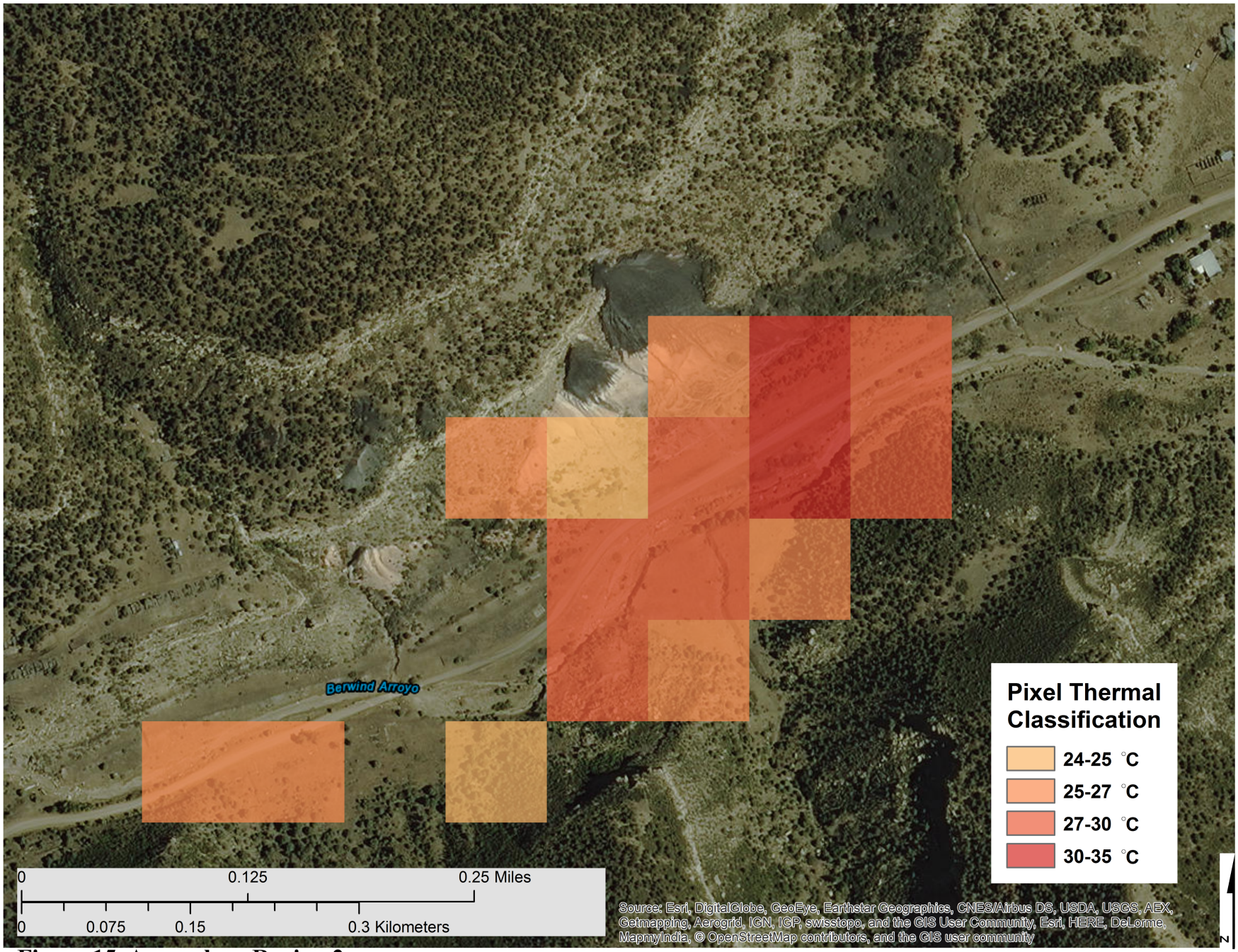

Figure 15. Anomalous Region 2.

Overlay of anomalous region with high-resolution basemap. The thermal anomalies may be coming from the surfaces with higher thermal inertia present in the image. Coal mine tailings present in this location could be retaining insolation longer, throwing of temperature calculations. Notice the thermal pixels are shifted south and east of the coal mine tailing. This overlay issue is likely resulting from differences in spatial resolution between the basemap and the ASTER pixels. This error could not be corrected as the basemap is housed on an Esri server.